Published for SISSA by Springer

Received: October 30, 2023
Revised: December 21, 2023
Accepted: January 22, 2024
Published: February 8, 2024

Sommerfeld effect for continuum gamma-ray spectra from Dark Matter annihilation

Barbara Jäger and Martin Vollmann

Institute for Theoretical Physics, University of Tübingen, Auf der Morgenstelle 14, 72076 Tübingen, Germany

E-mail: jaeger@itp.uni-tuebingen.de, martin.vollmann@itp.uni-tuebingen.de

Abstract: We present a calculation of the continuum part of the gamma-ray spectra resulting from Dark Matter annihilation in the framework of the MSSM taking into account Sommerfeld effects. Concentrating on pure wino and pure higgsino scenarios we compare our calculation to existing work and explore the numerical impact of the features not captured by previous approximative descriptions. We find that, in particular for large neutralino masses, when the Sommerfeld enhancement is very large, chargino-antichargino annihilation processes, which have not been considered before, lead to sizable differences with respect to existing calculations. In scenarios with neutralinos in the intermediate-mass range, we find that the role of the charginos is crucial in the endpoint regime. Our calculation provides the currently most accurate prediction for the continuum gamma-ray spectra.

Keywords: Higher Order Electroweak Calculations, Particle Nature of Dark Matter, Supersymmetry

ArXiv ePrint: 2310.11067

https://doi.org/10.1007/JHEP02(2024)051

JHEP02(2024)051

Contents

1 Introduction

Understanding the nature and origin of Dark Matter (DM) represents one of the great challenges of contemporary research in cosmology, astro- and particle physics. While there is little doubt in the community on the very existence of such a form of matter that does not interact electromagnetically with ordinary matter, the Standard Model of particle physics (SM) does not offer an obvious candidate particle to account for it.

Promising DM candidates are provided by models of physics beyond the SM (BSM) featuring weakly interacting massive particles (WIMPs) with masses in the range of a few hundred GeV to a few TeV. It is assumed that after a period of equilibrium between thermal WIMP production and annihilation in the early Universe a freeze-out of their number density occurred when the expansion rate of the Universe became larger than the relevant interaction rate. The measured abundance of DM is compatible with the existence of a WIMP at the electroweak (EW) mass scale.

A natural framework for WIMPs is provided by supersymmetric theories that complement the particle spectrum of the SM by so-called superpartners with spin differing by one half. The breaking of supersymmetry (SUSY) allows these particles to acquire masses different

JHEP02(2024)051

from their SM partners. In many SUSY models the lightest stable particle (LSP) represents a viable DM candidate. A prime example of such a model is constituted by the Minimal Supersymmetric Standard Model (MSSM). The MSSM contains a minimum number of SUSY particles, i.e. one superpartner for each SM particle apart from the Higgs boson. The Higgs sector has to be extended, resulting in five physical bosonic Higgs states and the same number of fermionic higgsinos. Form a theoretical point of view, the MSSM is appealing not only because of its underlying symmetry structure, but also by ensuring the unification of gauge couplings, naturalness, and providing a DM candidate. In most realizations of the MSSM the lightest neutralino, which effectively is a mixture of bino, wino and higgsino components, is considered stable and thus constitutes a viable WIMP DM candidate.

Great hopes for the discovery of SUSY particles were pinned on the CERN Large Hadron Collider (LHC) with the highest collision energies ever achieved on Earth by a proton accelerator. Dedicated searches by the ATLAS and CMS experiments put limits on the MSSM parameter space, but still leave room for the existence of SUSY particles, in particular in so-called *split* scenarios where the LSP is much heavier than the scale of EW symmetry breaking [1–3]. In such scenarios neutralino mixing effects are typically suppressed and the DM candidate is part of a "pure" EW multiplet [4]. Such scenarios are appropriately referred to as *higgsino* or *wino* type. Due to the large neutralino masses these DM models predict they remain elusive to searches at colliders and direct detection experiments.

Depending on the underlying model, DM candidates are supposed to be produced in pairs or in association with accompanying particles in collisions of SM particles [5, 6]. If the masses of the DM particles are large and/or their interactions with SM particles feeble, the corresponding production rates are low. The same limitation applies to direct detection experiments that aim to identify the recoil of a DM particle off a nuclear target [7–10].

Promising alternatives for DM searches in such scenarios are constituted by indirect detection strategies aiming at identifying annihilation signatures of DM particles [11, 12]. In particular, when such annihilation processes are accompanied by photon emission the resulting gamma ray spectra feature a very characteristic peak structure at the kinematical endpoint. The shape and intensity of such spectra can be heavily influenced by the so-called *Sommerfeld effect* [13–15]. This, in turn, can be exploited to overcome severe limitations of indirect searches due to large uncertainties in the distribution of DM in the inner galaxy and omni-present astrophysical backgrounds. The Sommerfeld effect is ubiquitous in annihilation processes involving non-relativistic particles that can exhibit long-range interactions. This phenomenon applies to MSSM neutralinos, where the long-range interactions are mediated by electroweak bosons.

A plethora of experiments and astrophysical observations has been devised to make use of this detection strategy. Particularly interesting for indirect neutralino searches are various observatories. These include the space telescope Fermi-LAT [16] which is suitable for neutralino searches in the mass range of $\mathcal{O}(1) - \mathcal{O}(100)$ GeV. Additional information is coming from the currently operating Imaging Air Cherenkov Telescopes H.E.S.S. [17], VERITAS [18], MAGIC [19], along with their next-generation counterparts CTA [20] and LHAASO [21]. The water Cherenkov telescope HAWC [22] further enriches this list. These Cherenkov telescopes are particularly suited for neutralino searches with somewhat heavier masses in the range of $\mathcal{O}(0.1) - \mathcal{O}(100)$ TeV.

JHEP02(2024)051

Specific SUSY searches using gamma-ray observations have been conducted in refs. [23–29] while in refs. [30–35] similar searches and predictions have been presented for more generic WIMP hypotheses.

From the theoretical point of view, exploiting the full potential of this search strategy requires a quantitative understanding of the Sommerfeld effect. In the context of the *full* MSSM, work to that effect has been limited. In particular, refs. [23, 26] are, to our knowledge, the only papers including the Sommerfeld enhancement in their MSSM analyses. In these studies, however, the incorporation of the Sommerfeld effect is achieved through the matching of exclusive 2-to-2 Sommerfeld-resummed neutralino-annihilation cross sections. This approach has some caveats and, as we will argue, cannot account for several pivotal phenomenological aspects that can become crucial for future analyses.

We aim to fill that gap with this work. In particular, we compute *all* neutralino and chargino annihilation cross sections into three-body final states that are relevant for obtaining the continuum gamma-ray spectra. We obtain these annihilation cross sections in analytical form for arbitrary spin and helicity combinations of the final-state particles.

While our results are valid for generic MSSM parameter sets, for our numerical discussion we focus on the pure wino and higgsino limits. We find that the impact of the Sommerfeld effect on the continuum spectrum is sizable even when the neutralino mass is of the order of a few hundred GeV. Our results show that, besides the Sommerfeld effect being very large [36], the chargino contribution dominates for the intermediate to the very high energy part of the gamma-ray spectrum. This aspect has not been captured by previous computations.

The paper is structured as follows: in section 2 we briefly review the basic theoretical aspects of indirect DM detection using gamma rays. We then move on to the discussion of the Sommerfeld effect in the context of SUSY and the methods we used for the calculation of annihilation cross sections in section 3. In section 4 we discuss our numerical results in the context of pure wino and higgsino scenarios, and we then conclude in section 5. Conventions and some technical aspects of our work are discussed in appendix A and appendix B.

2 The gamma-ray emission spectrum resulting from neutralino annihilation

DM halos of nearby galaxies feature characteristic gamma-ray emission signals with an associated flux

$$\frac{\mathrm{d}\Phi}{\mathrm{d}E_\gamma} = \frac{1}{8\pi m_\chi^2} J_{\mathrm{obs}} \left\langle \frac{\mathrm{d}(\sigma v)}{\mathrm{d}E_\gamma} \right\rangle , \tag{2.1}$$

where J_{obs} is the astrophysical "J" factor [37] for a given observed region and $\langle \mathrm{d}(\sigma v)/\mathrm{d}E_\gamma \rangle$ is the velocity-averaged annihilation cross section of two DM candidate particles χ of mass m_χ into gamma rays. With some rare exceptions the J factors are independent of the gamma-ray energy E_γ, and are thus irrelevant for the description of the spectral properties of the DM gamma-ray signals, which are the focus of this work. We refer the reader interested in specific J factors to refs. [38–40] for the Milky Way and to refs. [41–43] for other astrophysical environments.

JHEP02(2024)051

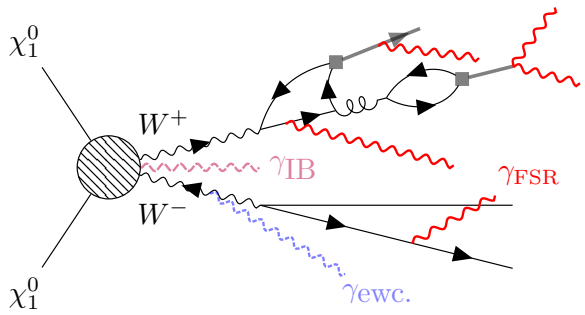

Figure 1. Illustrative Feynman diagram for the continuum contribution to the gamma-ray emission spectrum produced by neutralino annihilation. Red lines depict final-state photon radiation, blue lines soft/collinear electroweak radiation, and purple lines internal bremsstrahlung.

Here, however, we concentrate on the DM annihilation cross section $\mathrm{d}(\sigma v)/\mathrm{d}E_\gamma$ with the DM candidate particle being constituted by the lightest neutralino χ_1^0 of the MSSM. This annihilation cross section has a kinematic endpoint at $E_\gamma \simeq m_\chi$.[1] At this energy, the spectrum features a *quasi-monochromatic gamma-ray* line with a (natural) broadening of $\mathcal{O}(v^2)$, where v is the average speed of the neutralinos in the DM halos of interest ($v \approx 10^{-3}$ in the Milky Way). The monochromatic nature of the line is due to the two-body kinematics of the neutralino-annihilation process into photons, $\chi_1^0\chi_1^0 \to \gamma\gamma$. On top of the gamma-ray spectral line, the endpoint spectrum of neutralino annihilation involves a Z resonance (from the $\chi_1^0\chi_1^0 \to \gamma Z^*$ process) with a natural width of $\Gamma_Z/m_Z \sim 0.03$. Both the $\gamma\gamma$ and the γZ contributions at the endpoint of the spectrum are, in principle, loop suppressed. However, the narrow width of the Z resonance and the significant influence of long-range interactions between the neutralinos and the charginos due to the Sommerfeld effect make these features highly intriguing in terms of detectability.

The remaining part of the spectrum, *the continuum*, is generated by the sum of all processes where neutralinos annihilate into a gamma-ray photon in association with a multiparticle configuration "X", i.e. $\chi_1^0\chi_1^0 \to \gamma + X$. At leading order (LO) in the electroweak coupling, X consists of two SM particles. For clarity, we use a superscript in order to differentiate such a two-body state $X^{(2)}$ from the more complex sub-states X that can occur in general, and that are illustrated by figure 1.

In many simulations, such continuum configurations are approximated by matching fixed-order computations for two-particle production processes to parton-shower programs such as `Pythia` [44] or `Herwig` [45]. In this approach gamma-ray spectra from WIMP annihilation are obtained using the parton-shower approximation formula

$$\frac{\mathrm{d}(\sigma v)}{\mathrm{d}E_\gamma} \approx \sum_{X^{(2)}} (\sigma v)_{X^{(2)}} \frac{\mathrm{d}N^{\mathrm{MC}}_{X^{(2)}\to\gamma}}{\mathrm{d}E_\gamma}\,, \tag{2.2}$$

where, given a specific WIMP model, the coefficients $(\sigma v)_{X^{(2)}}$ are the (tree-level) cross sections for the annihilation of two DM candidate particles into two SM particles (e.g. $X^{(2)} = b\bar{b}, \tau^+\tau^-, W^+W^-, \ldots$), while the model-independent functions $\mathrm{d}N^{\mathrm{MC}}_{X^{(2)}\to\gamma}/\mathrm{d}E_\gamma$ for the

[1] We use natural units: $\hbar = c = 1$.

JHEP02(2024)051

gamma-ray emission off the SM particles are obtained from the aforementioned Monte-Carlo event generators.[2] These functions are available in specialized software packages such as `DarkSUSY` [46], PPPC [47] or `MicrOMEGAs` [48].

As a diagrammatic visualization, in figure 1 we show an example of a Feynman diagram for the continuum contribution to the gamma-ray emission spectrum produced by neutralino annihilation. From that particular diagram only those photon lines that are emitted from final-state legs are accounted for by the early implementations of eq. (2.2) (e.g. `DarkSUSY` versions before `v5` [49]). Such contributions are termed *final-state radiation* (FSR). Soft/collinear electroweak radiation effects have also been included in the literature (see, e.g., ref. [50]). In particular, the fragmentation functions provided by the PPPC code include these corrections. Newer versions of `DarkSUSY` instead provide a more complete picture for the neutralino-annihilation photon spectrum at the expense of losing the model-independence of eq. (2.2). In addition to pure FSR calculations they capture potentially dominant processes such as the so-called *internal bremsstrahlung* (IB) [51–55], which is absent in the PPPC approach [47]. This is achieved by computing the full fixed-order $\chi_1^0\chi_1^0 \to \gamma + X^{(2)}$ annihilation cross section for a given state $X^{(2)}$ ($X^{(2)} = W^+W^-$ in the sample diagram of figure 1) and matching it to a parton-shower program while carefully subtracting redundant terms in order to avoid double counting, see e.g. ref. [54]. In particular, IB becomes important in those cases where the otherwise helicity-suppressed annihilation of non-relativistic Majorana particles into a particle-antiparticle pair of light fermions becomes sizable once radiation effects are accounted for. It has been even observed that in some WIMP models, IB gives the dominant contribution to the gamma-ray spectrum in the medium-to-high energy regime (see refs. [56–58] for more details).

3 Sommerfeld effect

The previous discussion evidences that great progress have been achieved in understanding the continuum part of the gamma-ray spectrum from neutralino annihilation. By combining fixed-order computations with Monte-Carlo event generators (see eq. (2.2)), a relatively adequate theoretical picture of the WIMP gamma-ray spectrum can be obtained. This picture, however, fails at capturing *virtual* (loop) effects which, as we will see below, can become crucial. In particular, multi-loop corrections such as the one depicted in figure 2 can have an enormous impact on the annihilation cross sections of heavy neutralinos [36, 59, 60], resulting in enhancement factors of several orders of magnitude.

The primary reasons for this phenomenon are (A) the non-relativistic nature of the initial state consisting of two neutralinos, (B) t-channel interactions between them mediated by the gauge and Higgs bosons of the theory (see sketch in figure 2), and (C) the fact that these exchange bosons are lighter than the annihilating neutralinos. These features make a quantum-mechanical approach in terms of static potentials the most appropriate in order to account for the self-interactions of the neutralinos prior to their annihilation. In more formal terms, the computation of Feynman diagrams such as the one depicted in figure 2 will

[2] In the leading-logarithmic approximation of the aforementioned event generators, the fragmentation of the two SM particles is considered independently. This implies that $\mathrm{d}N^{\mathrm{MC}}_{X^{(2)}\to\gamma}/\mathrm{d}E_\gamma$ in eq. (2.2) actually denotes the sum of two fragmentation functions — one for each leg of primaries in figure 1.

JHEP02(2024)051

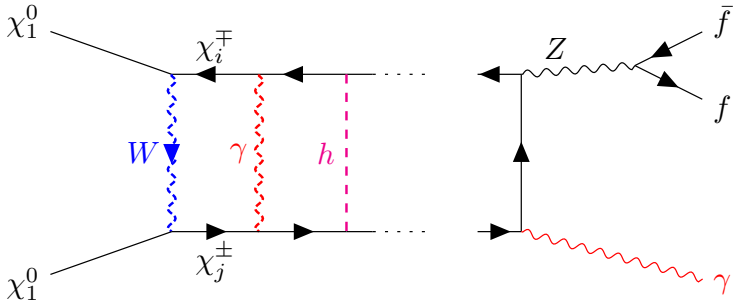

Figure 2. Prototypical ladder-like Feynman diagram contributing to the Sommerfeld effect.

inevitably yield terms that are (parametrically)[3] of $\mathcal{O}(\alpha^n m_\chi^n / m_W^n)$, where n is the number of loops in the given ladder-like diagram and α denotes the fine structure constant. Therefore, since we assume that $m_W \ll m_\chi$, the contribution of each of these diagrams is large and cannot be neglected. Rather all such terms need to be systematically *resummed*.

The resummation of these diagrams can be performed consistently in the context of non-relativistic effective field theories (NREFTs) [61] (in the context of MSSM neutralino annihilations, see e.g. refs. [62–64]) *independently of the exclusiveness* of the final state. For the particular case of neutralino annihilation into photons, the resulting annihilation cross section is given by [65, 66]

$$\frac{\mathrm{d}(\sigma v)}{\mathrm{d}E_\gamma} = 2 \sum_{IJ} S_{IJ} \left[\frac{\mathrm{d}(\tilde{\sigma} v)}{\mathrm{d}E_\gamma} \right]_{IJ} , \tag{3.1}$$

where S_{IJ} is the matrix of the so-called *Sommerfeld factors*, and we will refer to $\mathrm{d}(\tilde{\sigma v})/\,\mathrm{d}E_\gamma$ as the *annihilation matrix* for the Sommerfeld-corrected $\chi_1^0\chi_1^0 \to \gamma + X$ process. The pair indices I, J denote all possible neutral combinations of neutralino-neutralino and chargino-antichargino pairs within the MSSM [64]. There are 14 such combinations:

$$\begin{aligned} &\{(\chi_1^0\chi_1^0), (\chi_1^0\chi_2^0), (\chi_1^0\chi_3^0), (\chi_1^0\chi_4^0), (\chi_2^0\chi_2^0), (\chi_2^0\chi_3^0), (\chi_2^0\chi_4^0), (\chi_3^0\chi_3^0), (\chi_3^0\chi_4^0), (\chi_4^0\chi_4^0), \\ &(\chi_1^+\chi_1^-), (\chi_1^+\chi_2^-), (\chi_2^+\chi_1^-), (\chi_2^+\chi_2^-)\} . \end{aligned} \tag{3.2}$$

We compactly denote each pair index K by nested particle indices distinguishing between neutralino and chargino states using either round or angular brackets, i.e. $K = \{(\hat{ij})\}$, where $(\hat{ij}) = (\hat{11}), (\hat{12}), \ldots$ for the four neutralinos $(i, j = 1, \ldots, 4)$ and $K = \{\langle x\bar{y}\rangle\}$, with $\langle x\bar{y}\rangle = \langle 1\bar{1}\rangle, \langle 1\bar{2}\rangle, \ldots$ for the two charginos $(x, y = 1, 2)$. Note that while the neutralino states satisfy $(\hat{ji}) = (\hat{ij})$, the chargino states are not exchange symmetric ($\langle y\bar{x}\rangle \neq \langle x\bar{y}\rangle$).

Figure 3 captures the essence of eq. (3.1) in the representative $\chi_1^0\chi_1^0 \to \gamma + f\bar{f}$ process. In that particular example, the corresponding (interference) term of the equation with $I = \langle x\bar{y}\rangle$ and $J = (\hat{ij})$ is shown. The diagram explicitly illustrates that both the Sommerfeld factors and the annihilation matrix elements can be expressed as products of quantities corresponding to the intermediate states I and J, respectively. In the calculation of the annihilation matrix elements, the amplitudes of the $\chi_x^+\chi_y^- \to \gamma + f\bar{f}$ and the (complex

[3] Note that the parameters $v\, m_\chi$, m_Z, m_W, m_h are assumed to be of the same order of magnitude, and much smaller than m_χ.

JHEP02(2024)051

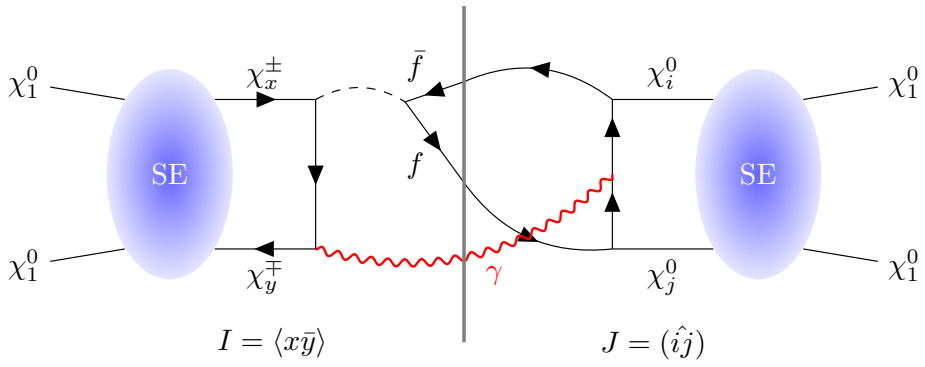

Figure 3. Sketch of a typical term in the Sommerfeld resummation formula of eq. (3.1) for the representative $\chi_1^0\chi_1^0 \to \gamma + f\bar{f}$ process.

conjugated) $\chi_i^0\chi_j^0 \to \gamma + f\bar{f}$ processes enter. For the computation of the S_{IJ} factors quantum mechanical wave functions evaluated at the spatial origin have to be multiplied with their complex conjugates. These wavefunctions describe the non relativistic $\chi_1^0\chi_1^0 \xrightarrow{\text{SE}} \chi_x^+\chi_y^-$ and (complex conjugated) $\chi_1^0\chi_1^0 \xrightarrow{\text{SE}} \chi_i^0\chi_j^0$ transitions as we briefly discuss in the following.

3.1 Computation of the Sommerfeld factors

Up to corrections of $\mathcal{O}(v^2)$ and $\mathcal{O}(m_W^2/m_\chi^2)$, the resummation of ladder-like diagrams such as the ones shown in figure 2 requires solving the following matrix Schrödinger equation[4] for the multicomponent function $u_{IK}(r)$ [64]

$$-\frac{1}{m_\chi}\frac{\mathrm{d}^2 u_{IK}}{\mathrm{d}r^2}(r) + \sum_J \left[\Delta M + V(r)\right]_{IJ} u_{JK}(r) = m_\chi v^2 u_{IK}(r)\,, \tag{3.3}$$

$$u_{IK}(r=0) = 0\,, \qquad \frac{\mathrm{d}u_{IK}(r=0)}{\mathrm{d}r} = \delta_{IK}\,. \tag{3.4}$$

The Sommerfeld factors S_{IJ} in eq. (3.1) are then given by

$$S_{IJ} = U^{*\,-1}_{I(\hat{1}\bar{1})} U^{-1}_{J(\hat{1}\bar{1})}\,, \tag{3.5}$$

where

$$U_{IK} = \lim_{r\to\infty}\left[\mathrm{e}^{ik_I r}\left(\frac{\mathrm{d}u_{IK}(r)}{\mathrm{d}r} - ik_I u_{IK}(r)\right)\right]\,, \tag{3.6}$$

$k_I \equiv \sqrt{m_\chi^2 v^2 - m_\chi(M_I - 2m_\chi)}$ and M_I is the sum of the masses of the non-relativistic "I" state, e.g. $M_{\langle 1\bar{2}\rangle} = m_{\chi_1^\pm} + m_{\chi_2^\pm}$.

The potential matrix in terms of the "coupling matrices" $\hat{\alpha}_{IJ}^B$ is given by

$$V_{IJ}(r) = \begin{pmatrix} \displaystyle\sum_{B^0=\gamma,Z,h,H^0,A^0} \hat{\alpha}^{B^0}_{(\hat{ij}),(\hat{kl})}\frac{\mathrm{e}^{-m_{B^0}r}}{r} & \displaystyle\sum_{B^+=W,H^+} \hat{\alpha}^{B^+}_{(\hat{ij}),\langle z\bar{w}\rangle}\frac{\mathrm{e}^{-m_{B^+}r}}{r} \\ \displaystyle\sum_{B^+=W,H^+} \hat{\alpha}^{B^+}_{\langle x\bar{y}\rangle,(\hat{kl})}\frac{\mathrm{e}^{-m_{B^+}r}}{r} & \displaystyle\sum_{B^0=\gamma,Z,h,H^0,A^0} \hat{\alpha}^{B^0}_{\langle x\bar{y}\rangle,\langle z\bar{w}\rangle}\frac{\mathrm{e}^{-m_{B^0}r}}{r} \end{pmatrix}\,, \tag{3.7}$$

[4]Here we are implicitly exploiting that in the partial-wave decomposition of the non-relativistic wave functions the contribution of states with non-vanishing orbital momentum ($\ell \neq 0$) is suppressed by factors of order $\mathcal{O}(v^{2\ell})$. We thus only retain contributions with $\ell = 0$.

JHEP02(2024)051

while the "mass-splitting" matrix ΔM in the basis of eq. (3.2) reads

$$\Delta M = \mathrm{diag}(0, m_{\chi_1^0} + m_{\chi_2^0} - 2m_\chi, \ldots, m_{\chi_1^\pm} + m_{\chi_2^\pm} - 2m_\chi, 2\,m_{\chi_2^\pm} - 2m_\chi)\,.$$

The Coulomb part of the potential ($B = B^0 = \gamma$) satisfies

$$\hat{\alpha}^\gamma_{(\hat{ij}),(\hat{kl})} = 0\,, \quad \text{and} \quad \hat{\alpha}^\gamma_{\langle x\bar{y}\rangle,\langle z\bar{w}\rangle} = \alpha\,\delta_{xz}\delta_{yw}, \tag{3.8}$$

where α is the fine-structure constant. The remaining coupling matrices depend on the MSSM parameters through the neutralino and chargino mixing matrices defined in eqs. (A.1)–(A.2) of appendix A. These had been already obtained in ref. [64], and we re-derived them using the conventions of ref. [67] that we use throughout this work. In the Feynman gauge the entries of these coupling matrices read

$$\hat{\alpha}^Z_{(\hat{ij}),(\hat{kl})} = \frac{1}{\sqrt{2}^{\delta_{ij}}}\frac{1}{\sqrt{2}^{\delta_{kl}}}\frac{\alpha}{s_W^2}\left[v^{Z\,(0)}_{ik}v^{Z\,(0)\,*}_{jl} - 3\,a^{Z\,(0)}_{ik}a^{Z\,(0)\,*}_{jl} + s^{G_Z\,(0)}_{ik}s^{G_Z\,(0)\,*}_{jl} + (k \leftrightarrow l)\right], \tag{3.9}$$

$$\hat{\alpha}^Z_{\langle x\bar{y}\rangle,\langle z\bar{w}\rangle} = \frac{\alpha}{s_W^2}(v^Z_{xz}v^{Z\,*}_{yw} - 3\,a^Z_{xz}a^{Z\,*}_{yw} + s^{G_Z}_{xz}s^{G_Z\,*}_{yw}), \tag{3.10}$$

$$\hat{\alpha}^W_{(\hat{ij}),\langle z\bar{w}\rangle} = \frac{1}{\sqrt{2}^{\delta_{ij}}}\frac{\alpha}{s_W^2}\left[v^W_{iz}v^{W\,*}_{jw} - 3\,a^W_{iz}a^{W\,*}_{jw} + s^{G_W}_{iz}s^{G_W\,*}_{jw} + (z \leftrightarrow w)\right], \tag{3.11}$$

for the vector mediators Z and $W^\pm$ and

$$\hat{\alpha}^S_{(\hat{ij}),(\hat{kl})} = \frac{1}{\sqrt{2}^{\delta_{ij}}}\frac{1}{\sqrt{2}^{\delta_{kl}}}\frac{\alpha}{s_W^2}\left[s^{S\,(0)}_{ik}s^{S\,(0)\,*}_{jl} + (k \leftrightarrow l)\right], \tag{3.12}$$

$$\hat{\alpha}^S_{\langle x\bar{y}\rangle,\langle z\bar{w}\rangle} = \frac{\alpha}{s_W^2}s^S_{xz}s^{S\,*}_{yw}\,, \tag{3.13}$$

$$\hat{\alpha}^{H^\pm}_{(\hat{ij}),\langle z\bar{w}\rangle} = \frac{1}{\sqrt{2}^{\delta_{ij}}}\frac{\alpha}{s_W^2}\left[s^{H^\pm}_{iz}s^{H^\pm\,*}_{jw} + (z \leftrightarrow w)\right], \tag{3.14}$$

for the scalar and pseudoscalar mediators, where S collectively labels all physical neutral Higgs bosons ($S = h, H, A^0$) in the MSSM, and the would-be Goldstone bosons G_Z, G_W associated with the Z and W bosons.

Explicit expressions for all the coefficients v^B_{IJ}, a^B_{IJ} and s^B_{IJ} can be found in appendix A. We obtained these by using the `Mathematica` [68] packages `FeynArts` [69] and `FormCalc` [70, 71] with the MSSM model file [67]. At the relevant perturbative order, our potential agrees with the corresponding results of ref. [64].

3.2 Computation of the annihilation matrices

In the previous section we briefly reviewed the NREFT methods that are necessary in order to properly incorporate the Sommerfeld effect in the continuum spectrum prediction. In particular, eq. (3.1) provides us with an elegant prescription on how to deal with this problem. Given the Sommerfeld coefficients S_{IJ} which can be computed by solving a system of Schrödinger equations, we need to determine the $[\mathrm{d}(\tilde{\sigma v})/\mathrm{d}E_\gamma]_{IJ}$ functions for every possible combination I, J. The IJ element of the annihilation matrix is defined by

$$\left[\frac{\mathrm{d}(\tilde{\sigma v})}{\mathrm{d}E_\gamma}\right]_{IJ} = \frac{1}{(\sqrt{2})^{\mathrm{id}(I)+\mathrm{id}(J)}}\frac{1}{4m_\chi^2}\sum_X\int \mathrm{d}\Pi'_{\gamma+X}\,\delta\left(E_\gamma - E'_\gamma\right)\mathcal{A}^{(\ell,s)=(0,0)}_{I\to\gamma+X}\mathcal{A}^{(\ell,s)=(0,0)\,*}_{J\to\gamma+X}\,, \tag{3.15}$$

JHEP02(2024)051

where the identical-particle index $\mathrm{id}(K) = \delta_{ij}$ for neutralino pairs [$K = (\hat{ij})$] or 0 for chargino-antichargino pairs [$K = \langle x\bar{y}\rangle$]. $\mathrm{d}\Pi'_{\gamma+X}$ is the phase-space integration element for the $\gamma + X$ final state, and $\mathcal{A}^{(\ell,s)=(0,0)}_{K\to\gamma+X}$ is the amplitude for the *s-wave annihilation*[5] of the two-particle state K into a $\gamma + X$ state. It is implicitly understood that the sum over X includes all possible spin and helicity combinations of the particles that are produced in association with the gamma ray.

In this article we compute the annihilation matrices of eq. (3.15) for the production of a photon in association with any possible combination of two SM particles $X = X^{(2)}$. Concretely, in the MSSM the only possible combinations are[6]

$$X^{(2)} = \{W^+W^-, W^\pm H^\mp, H^+H^-, ZS, SS', f\bar{f}\}\,, \tag{3.16}$$

where S and S' are shorthand for two different neutral Higgs scalars in the MSSM and $f\bar{f}$ denotes any fermion anti-fermion pair within the SM. There are $14 \times (14+1)/2 = 105$ independent symmetric combinations of the initial-state indices (see eq. (3.2)). Thus, for each one of the aforementioned combinations of $X^{(2)}$ 105 independent matrix elements have to be computed. Out of these matrix elements, in the literature only one is available [54], corresponding to the neutralino-neutralino annihilation cross section with $I = J = (\hat{11})$. In this work we compute the annihilation matrices for the remaining 104 combinations of I, J.

State-of-the-art software packages such as `FeynArts` [69] or `FormCalc` [70, 71] are capable of computing differential cross sections in analytical form for annihilation processes within complicated models such as the MSSM. However, the problem at hand requires some extra processing for the s-wave projection of the I, J states and for computing the interference of amplitudes with different initial states.

We addressed these issues by obtaining raw amplitudes for the 2-to-3 scattering processes $\chi^0_i\chi^0_j \to \gamma + X^{(2)}$ of all possible $X^{(2)}$ states of eq. (3.16) with arbitrary spin and helicity combinations using `FeynArts 3.11`/`FormCalc 9.8` and the built-in MSSM model file of ref. [67]. We then processed these amplitudes in the framework of `Mathematica` [68] to obtain the desired interference contributions.

3.2.1 Annihilation matrices in the FSR approximation

The calculation of the annihilation matrix $\mathrm{d}(\tilde{\sigma v})/\,\mathrm{d}E_\gamma$ presented above is *exact* at LO in the electroweak couplings. Thus, when multiplied with the Sommerfeld factors and matched with parton-shower simulations, the resulting prediction offers the most accurate description of the continuum gamma-ray spectrum from annihilating neutralinos up to the present day. However, an *approximate* treatment that exploits the fact that the computation of the Sommerfeld factors is independent of the exclusiveness of the final state in the annihilation process, is also possible and has already been considered in refs. [23, 26]. In that approach,

[5] A crucial point in eq. (3.15) is the fact that both the I and J states individually exhibit the same quantum numbers as the (physical) initial state of the system, $\chi^0_1\chi^0_1$. In the partial-wave basis this is the s-wave state with vanishing orbital ($\ell = 0$) and spin ($s = 0$) quantum numbers in virtue of the Majorana nature of the MSSM neutralinos, provided that $v \to 0$.

[6] The processes $\chi^0_1\chi^0_1 \to \gamma + ZZ$, $\gamma + \gamma Z$ and $\gamma + \gamma\gamma$ are forbidden because of the Landau-Yang theorem.

JHEP02(2024)051

eq. (2.2) generalizes to

$$\frac{\mathrm{d}(\sigma v)}{\mathrm{d}E_\gamma} \approx \sum_{X^{(2)}} (\sigma v)^{\mathrm{SE}}_{X^{(2)}} \frac{\mathrm{d}N^{\mathrm{MC}}_{X^{(2)}\to\gamma}}{\mathrm{d}E_\gamma}\,, \tag{3.17}$$

where, in analogy to eq. (3.1), the Sommerfeld-corrected 2-to-2 annihilation cross section is given by

$$(\sigma v)^{\mathrm{SE}}_{X^{(2)}} = 2\sum_{IJ} S_{IJ}\,(\tilde{\sigma v})^{X^{(2)}}_{IJ}\,, \tag{3.18}$$

and, as just argued, the fragmentation functions remain the same as in eq. (2.2). Eq. (3.17) is sensitive to the different polarizations of the 2-body final states. To emphasize this feature, the polarization states can be indicated explicitly as

$$\begin{aligned} X^{(2)} = \{&W_T^+W_T^-, W_\odot^+W_\odot^-, W_L^\pm H^\mp, f_L\bar{f}_L, f_R\bar{f}_R, f_L\bar{f}_R, f_R\bar{f}_L, \gamma_T\gamma_T, \gamma_T Z_T, Z_T Z_T,\\ &Z_\odot Z_\odot, Z_\odot S, SS'\}\,, \end{aligned}$$

where the subscripts "T" and "$\odot$" refer to their transverse and longitudinal polarization components of the gauge bosons and the "L" and "R" subscripts denote the left- and right-handed chirality of the fermions, respectively. While the unpolarized cross sections for these 2-body states are already known [62], we obtain the polarized ones for the first time in this work.

4 Numerical results

In light of the inherent complexity of the MSSM, a thorough exploration of our calculations requires a dedicated study. In this section, we focus on two limiting scenarios of the MSSM: the pure wino and the pure higgsino case. These models have been investigated intensively in the last several years (see e.g. [23, 59, 72–76]). We note that even in the most generic MSSM parameter sets, the Sommerfeld effect has a significant impact on the associated indirect detection signals.

The most general form of the softly broken MSSM introduces 105 parameters in addition to those present in the SM [77]. These are interdependent given a specific supersymmetry breaking scenario. Current experimental efforts to search for SUSY, however, concentrate on constrained versions of the MSSM such as the 18-parameter phenomenological MSSM (pMSSM) [78] or the 4-parameter constrained MSSM (CMSSM) (see, e.g., refs. [27, 79]). The pMSSM, for example, treats the mass terms for gauginos (M_1, M_2, M_3), higgsino ($\pm|\mu|$), sfermions and trilinear couplings, as well as the ratio of the vacuum-expectation values of the two Higgs doublets ($\tan\beta$), as independent parameters.

In the pure wino and higgsino limits, the sfermion masses as well as the trilinear couplings, the gluino mass parameter M_3, and $\tan\beta$ are assumed to be infinitely large. In the pure wino limit, in addition to integrating out the sfermions it is assumed that $M_1 \to \infty$ and $|\mu| \to \infty$, leaving M_2 as the only relevant MSSM parameter. In the spirit of the minimal DM models discussed in ref. [72] (see also refs. [80, 81] for a more recent study on minimal DM) the wino can be visualized as an SU(2) Majorana triplet which, after electroweak symmetry

JHEP02(2024)051

breaking, gives rise to one chargino and one neutralino degree of freedom. Similarly, the pure higgsino limit can be constructed by introducing an SU(2) Dirac doublet that results in two neutralinos and one chargino. Note that in these reduced scenarios, the Majorana (neutralino/chargino) and the scalar (two-Higgs doublet) sectors of the MSSM can not be coupled without explicitly breaking the electroweak symmetry. As a result, the Higgs parameters do not play any role in our predictions.

The pure wino and higgsino scenarios do not provide satisfactory solutions to the hierarchy problem and the unification of gauge couplings, which were among the primary motivations for introducing SUSY. Moreover, for sub-TeV neutralino masses within the standard freeze-out hypothesis they predict more DM than observed [4]. Nonetheless, these limiting scenarios serve as highly valuable toy models. For instance, the dimension of the Sommerfeld and the annihilation matrices in eq. (3.1) is reduced to two for the pure wino and to three for the pure higgsino model, respectively, thus significantly reducing the complexity of calculations and analyses as compared to the full MSSM.

For the numerical results shown below as electroweak input parameters we choose the mass of the Z boson,$m_Z = 91.1876\,\text{GeV}$, the Fermi constant, $G_\mu = 1.1663788 \times 10^{-5}\,\text{GeV}^{-2}$, and the fine structure constant, $\alpha_0 = 1/137.035999180$ as quoted by the Particle Data Group [82]. From these input parameters, the mass of the W boson, $m_W = 80.360\,\text{GeV}$, and the Weinberg angle $\sin^2\theta_W = 0.22338$ are obtained using the electroweak relations of ref. [82]. In our numerical implementations we use the running QED coupling evaluated at the scale m_Z, $\alpha = 1/128.93$. The masses of the u, d, s quarks, the electron and muon, and of all neutrinos are neglected. For the c, b, t quarks, the tau lepton, and the Higgs boson we use the masses quoted in ref. [82]: $m_c = 1.27\,\text{GeV}$, $m_b = 4.18\,\text{GeV}$, $m_t = 172.69\,\text{GeV}$, $m_\tau = 1.77686\,\text{GeV}$, and $m_h = 125.25\,\text{GeV}$. Finally, for the relative speed of the annihilating particles we use the nominal value of $v = 10^{-3}$, which translates into a velocity of ~ 300 km/s, which is a typical value in Milky-Way sized halos. Rather fortunately, our results are insensitive to this choice. This is because of a generic property of the Sommerfeld factor at low velocities ($v \lesssim m_W/m_\chi$) in the presence of Yukawa potentials: when the de Broglie wavelength $1/(m_\chi v)$ is much larger than the range of the (leading) Yukawa interaction $1/m_W$, the Sommerfeld coefficients become velocity-independent, see e.g. ref. [83].

For both, wino-like and higgsino-like models, we use the one-loop expressions given in refs. [72, 84] for the mass splitting between the chargino and the lightest neutralino, $m_{\chi_1^\pm} - m_{\chi_1^0}$. For the mass splitting between the two neutralinos in the pure higgsino scenario we use $m_{\chi_2^0} - m_{\chi_1^0} = 20\,\text{MeV}$ in all our examples, as done in ref. [85].

The numerical results that are reported below involve comparisons between different prescriptions and approximations. For simplicity we introduce the following acronyms:

- `'fixed_noSE'`: neutralino-pair annihilation into a $\gamma + X^{(2)}$ final state at tree-level with no Sommerfeld resummation at fixed order ($\mathcal{O}(\alpha^3)$), as provided in ref. [86]. Generally, $X^{(2)}$ denotes a two-particle state. In the pure wino and higgsino models, only $X^{(2)} = W^+W^-$ occurs.

JHEP02(2024)051

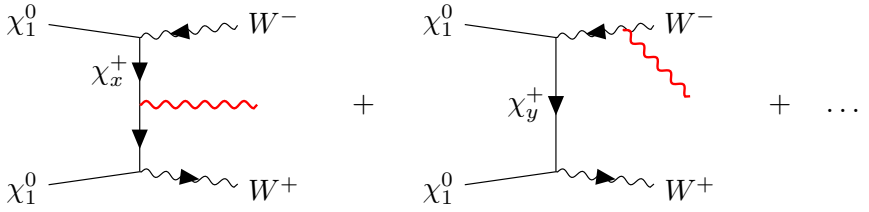

- `'FSR_SE'`: Sommerfeld-corrected neutralino-pair annihilation into a $\gamma + X^{(2)}$ final state where only photon emission due to FSR in the soft/collinear approximation is taken into account.

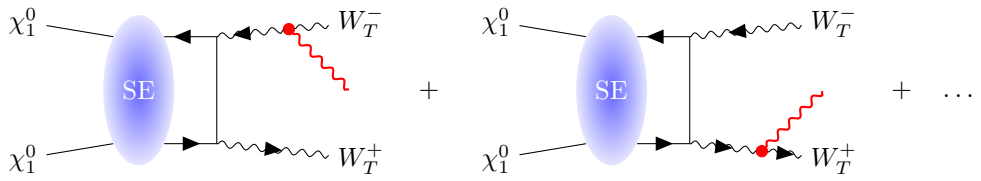

For the pure wino and higgsino scenarios, the only possible two-body final state is $X^{(2)} = W_T^+ W_T^-$. The spectrum that is obtained using this approximation is computed by using eq. (3.17) with the LO fragmentation function of ref. [50] which in this case assumes the particularly simple form

$$\frac{\mathrm{d}N_{W_T^+W_T^-}}{\mathrm{d}E_\gamma} = \frac{4}{m_\chi}\frac{\alpha}{\pi}\left\{\frac{E_\gamma}{m_\chi - E_\gamma}\left[\log\left(\frac{m_\chi - E_\gamma}{m_W} + \sqrt{\frac{(m_\chi - E_\gamma)^2}{m_W^2} - 1}\right)\right.\right. \\ \left.\left. + \left(\frac{m_\chi - E_\gamma}{E_\gamma} + \frac{E_\gamma(m_\chi - E_\gamma)}{m_\chi^2}\right)\log\frac{2\,m_\chi}{m_W}\right]\right\}. \tag{4.1}$$

- `'full_SE'`: neutralino-pair annihilation into a $\gamma + X^{(2)}$ final state including continuum contributions and Sommerfeld resummation effects. In contrast to the two previous approaches, this computation receives contributions from all the two-particle combinations of eq. (3.16).

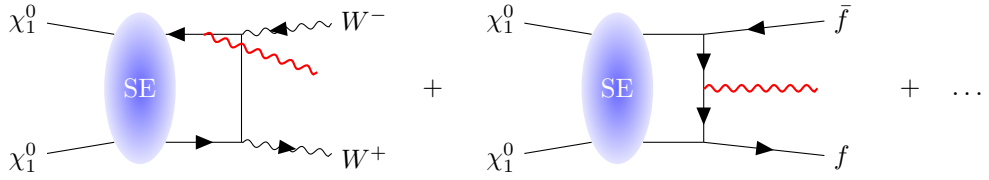

Note that the Sommerfeld-corrected spectral line contributions $\chi_1^0\chi_1^0 \to \gamma + X^{(1)}$ (where $X^{(1)} = \gamma$ or Z)[7] are not included in our results. These have already been studied extensively in the literature, e.g. see ref. [60] and references therein. Including these contributions is straightforward as they are proportional to Dirac delta functions centered at gamma-ray

[7] Our calculations do include a Z resonance feature (see our predicted spectra below) which, however, only capture processes of the type $\chi_1^0\chi_1^0 \to \gamma + Z^* \to \gamma + f\bar{f}$.

JHEP02(2024)051

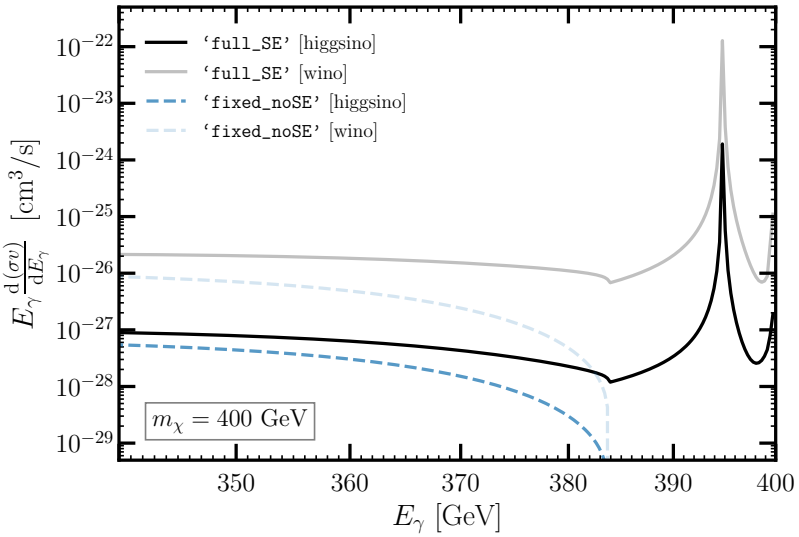

Figure 4. Gamma-ray spectrum of neutralino annihilation in the higgsino-like (black) and the wino-like (gray) scenarios with $m_\chi = 400$ GeV within our full calculation (solid lines) and the unresummed LO computation of ref. [86] (dashed lines).

energies $E_\gamma^{\gamma\gamma} = m_\chi$ and $E_\gamma^{\gamma Z} = m_\chi - m_Z^2/(4m_\chi)$, respectively. We nonetheless checked that the Sommerfeld-resummed neutralino annihilation cross sections into $\gamma\gamma$ (and γZ) agree with ref. [60] (e.g. Fig 5 therein), and are thus in agreement with fixed-order computations presented in refs. [87, 88] in the light ($m_\chi \sim 100\,\mathrm{GeV}$) pure wino/higgsino regime.

4.1 Scenarios with $m_\chi = 400\,\mathrm{GeV}$

In figure 4 we show the gamma-ray spectra of neutralino annihilation in these two scenarios for our full calculation including the Sommerfeld effect and compare it to the unresummed LO calculation of ref. [86]. Note that the results of the `'FSR_SE'` approach are zero in the plot range due to the kinematic threshold in eq. (4.1) at $E_\gamma \approx m_\chi - m_W \approx 320\,\mathrm{GeV}$. The comparison between the two remaining calculations illustrates impressively the relevance of the effects that have been neglected in the past, even when there are no large hierarchies between the masses of the lightest supersymmetric particles and the gauge bosons of the electroweak theory. The most striking peculiarity of figure 4 is the appearance of a resonance associated with a Z boson contribution which is omitted by the "naïve" fixed order computation. In particular, the fixed-order calculation has a clear cutoff from the kinematic threshold of the $\chi_1^0\chi_1^0 \to W^+W^-\gamma$ process at the energy $E_\gamma = m_\chi - m_W^2/m_\chi$ (corresponding to about 384 GeV in the scenarios of figure 4). The Sommerfeld-corrected continuum spectra `'full_SE'` that we compute here account for this Z-boson contribution by the inclusion of Feynman diagrams like the one shown in figure 2. In such diagrams fermion pairs can be created resonantly from a Z-boson in association with a photon with an energy that is larger than the aforementioned cutoff. The resulting peak of the Z resonance is then at $E_\gamma = m_\chi - m_Z^2/(4m_\chi)$, amounting to about 395 GeV in the scenarios of figure 4.

In addition to the Z resonance, the spectral region we uncovered in this work exhibits further interesting features. The almost imperceptible kinks around the $E_\gamma = m_\chi$ endpoint

JHEP02(2024)051

(400 GeV in the scenarios of this section) are due to the kinematic thresholds in the $\chi_1^0\chi_1^0 \to f\bar{f}\gamma$ processes, where f denotes any charged fermion of the SM with non-vanishing mass. For instance, the $\chi_1^0\chi_1^0 \to b\bar{b}\gamma$ process is only possible, if $E_\gamma < m_\chi - m_b^2/m_\chi$ ($= 399.96\,\text{GeV}$ in the current scenario).

The Sommerfeld effect in the spectral region that is covered by the original fixed-order computation of ref. [86], i.e. below the W^+W^- threshold, yields a significant enhancement. As the m_χ/m_W hierarchies become larger, the numerical impact becomes even more pronounced, as we shall discuss below. Independent of the neutralino mass, however, annihilation cross sections and Sommerfeld factors from wino-like neutralinos are generically larger than in the higgsino-like case, because the electroweak charges in the pure wino limit are a factor of two larger than those for the pure higgsino limit. For instance, the Born-level annihilation cross section of wino-like neutralinos into W^+W^- pairs is sixteen times larger than the corresponding cross section for higgsino-like neutralinos.

4.2 Scenarios with heavier neutralinos

Accounting for the Sommerfeld enhancement becomes more and more important as the mass of the neutralinos is increased. In figure 5 we demonstrate this numerically for higgsino- and wino-like scenarios with a lightest neutralino of mass 600 GeV and 2.4 TeV, respectively.

In each of these heavy neutralino scenarios, the predictions obtained within our full calculation show strong enhancements compared to the fixed-order computations. In the soft-photon part of the spectrum shown in figure 5 we observe how well the FSR predictions `'FSR_SE'` match our improved predictions `'full_SE'` and how this agreement improves, as expected, when m_χ is increased. In particular, due to the model-independence of the splitting function of eq. (4.1), the ratios of the Sommerfeld-resummed calculations `'FSR_SE'` to the fixed-order results `'fixed_noSE'` are roughly independent of E_γ as long as $E_\gamma \ll m_\chi$. In the higgsino-like scenario these ratios amount to an enhancement by a factor of about 1.5 for $m_\chi = 600\,\text{GeV}$ and of about 4.6 for $m_\chi = 2.4\,\text{TeV}$. In the wino-like scenario we find enhancement factors of ~ 1.9 for $m_\chi = 600\,\text{GeV}$ and of 990 for $m_\chi = 2.4\,\text{TeV}$.

This huge enhancement of the gamma-ray spectrum in the large-m_χ pure wino scenario is due to the resonant nature of the Sommerfeld effect (see e.g. figure 1 of ref. [36]). For particular neutralino masses the binding energy of a chargino-antichargino bound state is exactly zero, which ultimately results in a strong enhancement of the DM annihilation cross section. When varying the neutralino mass within our pure-wino scenario the enhancement factor reaches a first resonance at $m_\chi = 2.29\,\text{TeV}$.[8] It then decreases and increases again, until the second resonance is reached at $m_\chi = 8.83\,\text{TeV}$. Note that, as discussed e.g. in ref. [90], depending on the SUSY parameters, the Sommerfeld resummation can lead to suppressed rather than enhanced annihilation rates. Pure winos and higgsinos with resonantly enhanced cross sections are excluded by both Cherenkov and satellite telescopes even in the most conservative assumptions about the DM halos [75, 76]. Off-resonance neutralinos with masses of 600 GeV or 2.4 TeV considered here are still allowed provided the DM distribution in the center of the Galaxy is rather cored [75].

[8] The numerical value of the neutralino mass for which such resonance effects occur is very sensitive to the chargino-neutralino mass splitting, and also depends on NLO corrections to the non-relativistic potential, see e.g. ref. [89] and references therein.

JHEP02(2024)051

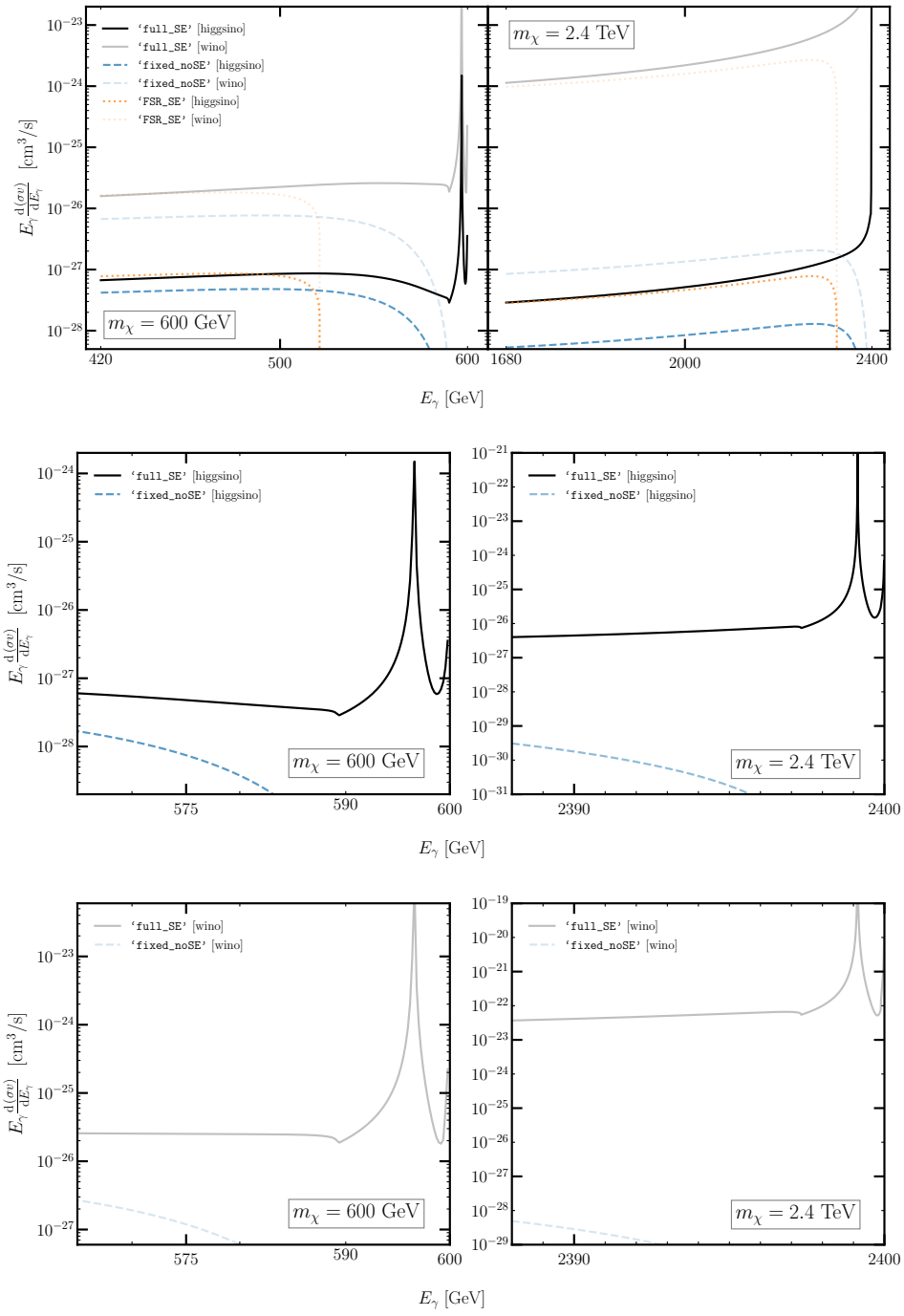

Figure 5. Upper panels: gamma-ray spectrum of neutralino annihilation in the higgsino-like (black) and the wino-like (gray) scenarios with $m_\chi = 600\,\mathrm{GeV}$ (left) and $m_\chi = 2.4\,\mathrm{TeV}$ (right) within our full calculation (solid lines), the unresummed LO computation of ref. [86] (dashed lines), and the collinear-approximated computation of ref. [50] (dotted orange lines). Middle panels: full calculation (solid lines) and unresummed LO computation (dashed lines) in the higgsino-like scenario close to the endpoint region. Lower panels: full calculation (solid lines) and unresummed LO computation (dashed lines) in the wino-like scenario close to the endpoint region.

JHEP02(2024)051

	$m_\chi = 400\,\text{GeV}$	$m_\chi = 600\,\text{GeV}$	$m_\chi = 2.4\,\text{TeV}$
$S_{(\hat{1}\hat{1})(\hat{1}\hat{1})}$	1.083	1.201	251.4
$S_{(\hat{1}\hat{1})\langle 1\bar{1}\rangle}$	0.265	0.449	348.0
$S_{\langle 1\bar{1}\rangle\langle 1\bar{1}\rangle}$	0.065	0.168	481.8

Table 1. Elements of the Sommerfeld matrix in the pure-wino limit of the MSSM for the three neutralino masses considered in this section.

As E_γ increases, the situation becomes even more intriguing, requiring us to consider the relative impact of the various entries in eq. (3.1) for unraveling the underlying dynamics. More specifically, in the pure wino limit eq. (3.1) can be decomposed into three terms:

$$\frac{\mathrm{d}(\sigma v)}{\mathrm{d}E_\gamma} = 2\,S_{(\hat{1}\hat{1})(\hat{1}\hat{1})}\left[\frac{\mathrm{d}(\tilde{\sigma v})}{\mathrm{d}E_\gamma}\right]_{(\hat{1}\hat{1})(\hat{1}\hat{1})} + 4\,\mathrm{Re}\left\{S_{(\hat{1}\hat{1})\langle 1\bar{1}\rangle}\left[\frac{\mathrm{d}(\tilde{\sigma v})}{\mathrm{d}E_\gamma}\right]_{(\hat{1}\hat{1})\langle 1\bar{1}\rangle}\right\} 2\,S_{\langle 1\bar{1}\rangle\langle 1\bar{1}\rangle}\left[\frac{\mathrm{d}(\tilde{\sigma v})}{\mathrm{d}E_\gamma}\right]_{\langle 1\bar{1}\rangle\langle 1\bar{1}\rangle}, \tag{4.2}$$

where a numerical evaluation of the Sommerfeld factors yields the results listed in table 1. In order to interpret the entries of the table, it is important to bear in mind that in the absence of the Sommerfeld effect $S_{IJ} = \delta_{I(\hat{1}\hat{1})}\delta_{J(\hat{1}\hat{1})}$. In the "low mass" scenario ($m_\chi = 400$ GeV), this condition is satisfied at the level of about 30%. This, for instance, explains why in figure 4, the deviations from the `'fixed_noSE'` with respect to the `'full_SE'` computations are not extremely large in the $E_\gamma \ll 320\,\text{GeV}$ spectral region. However, as noted before, the `'fixed_noSE'` calculation misses the Z resonance effect and all additional $f\bar{f}\gamma$ contributions resulting from the last term of eq. (4.2). As the neutralino mass increases, the numerical significance of this term as well as of the interference term (second term in eq. (4.2)) grows substantially. As shown below, the role of the charginos becomes more and more crucial as the neutralino mass is increased.

Our `'full_SE'` calculation exhibits an interesting phenomenon at gamma-ray energies that are somewhat smaller than the threshold energy of the $W^+W^-\gamma$ final state, $E_\gamma = m_\chi - m_W^2/m_\chi$. Specifically, unlike the relatively "soft cutoff" behavior that is observed in the `'fixed_noSE'` computation, the `'full_SE'` prediction exhibits a subtle additional enhancement followed by a sharper decline near the threshold. This additional enhancement becomes more pronounced as the neutralino mass is increased, as apparent from the two m_χ scenarios depicted in figure 5. In order to better understand this behavior, we introduce the "normalized" matrix elements for the $W^+W^-\gamma$ channel, which is the only annihilation channel with non-vanishing diagonal and off-diagonal matrix elements in the wino/higgsino scenarios,

$$\frac{\mathrm{d}N_{IJ}^{W^+W^-}}{\mathrm{d}x} \equiv \frac{m_\chi}{(\tilde{\sigma v})_{IJ}^{W^+W^-}}\frac{\mathrm{d}}{\mathrm{d}E_\gamma}(\tilde{\sigma v})_{IJ}^{W^+W^-\gamma}, \tag{4.3}$$

where $x \equiv E_\gamma/m_\chi$. These matrix elements are dimensionless and approach the LO fragmentation function of eq. (4.1) asymptotically for sufficiently large m_χ and small enough x. We

JHEP02(2024)051

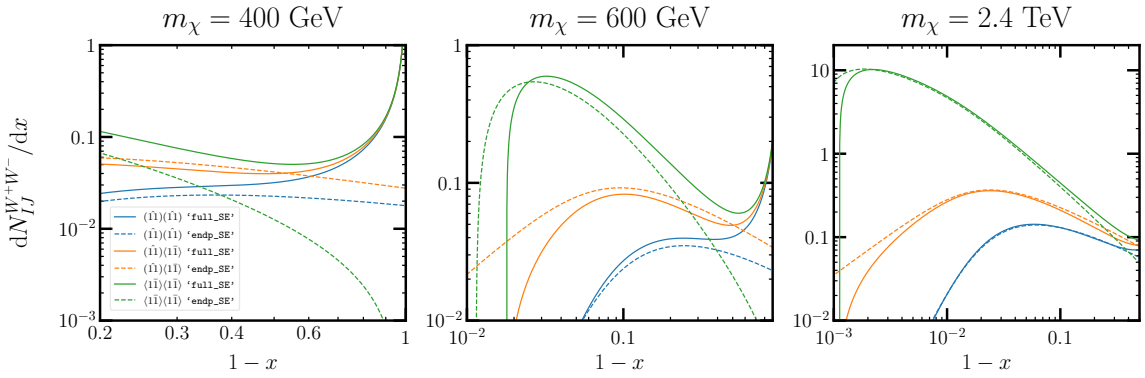

Figure 6. Comparison of the normalized matrix elements $\mathrm{d}N_{IJ}^{W^+W^-}/\mathrm{d}x$ in the pure wino model, as obtained using our `'full_SE'` calculation (solid lines), with the `'endp_SE'` calculations of refs. [91, 92] (dashed lines), as functions of $(1-x)$ for three different values of m_χ. Each color corresponds to the contribution of a single matrix element with indices IJ as introduced in section 3.

plot them in figure 6. We observe that in the regime $(1-x) \ll 1$ and for scenarios with heavy neutralinos, such as the considered case of $m_\chi = 2.4\,\mathrm{TeV}$, the diagonal matrix element with $I = J = \langle 1\bar{1}\rangle$ is much larger than the corresponding matrix elements for all other IJ combinations. In this case the three relevant Sommerfeld matrix elements S_{IJ} listed in table 1 are comparable in order of magnitude. We see that, when they are combined with the relevant annihilation matrix elements, the last term of eq. (4.2) in this scenario gives the dominant contribution in the $(1-x) \ll 1$ regime. The endpoint spectrum is thus dominated by virtual chargino annihilations. This is a consequence of the increasing influence of Sudakov logarithms for $(1-x) \ll 1$, which are particularly large for the terms of eq. (4.2) involving charginos.

Besides the Sommerfeld effect, which is the focus of this work, a different kind of resummation is necessary at *the endpoint region* of the spectrum. Indeed, for very heavy neutralinos and $E_\gamma \to m_\chi$ our `'full_SE'` computation suffers from large logarithmic enhancements that need to be incorporated (resummed) into the prediction. Such a resummation has already been completed for the MSSM in ref. [66] at the next-to-leading logarithmic (NLL) accuracy, while in refs. [65, 91] and [85] an NLL-prime (NLL') accuracy[9] was achieved for wino- and higgsino-like DM, respectively (see ref. [94] for a short review). The NLL' calculation exhibits an accuracy of $\mathcal{O}(1\%)$, while the accuracy of the NLL prediction is of order $\mathcal{O}(10\%)$. Similar calculations for wino-like DM can be found in ref. [95] at leading-logarithmic (LL) accuracy and ref. [96] (NLL), and for higgsino-like DM in ref. [97] (LL'), where all anomalous dimensions are given at 1-loop accuracy.

Indeed, we also verified that our results are consistent with the endpoint resummed calculation of refs. [85, 91, 92], to which we refer as `'endp_SE'` in the following, within their kinematic regimes of validity, namely, $m_\chi - E_\gamma \sim \mathcal{O}(m_W)$. For these comparisons an additional step is required. While in the `'endp_SE'` calculations, each annihilation-matrix element $[\mathrm{d}(\tilde{\sigma v})/\mathrm{d}E_\gamma]_{IJ}$ incorporates terms resummed to all orders in the electroweak coupling, annihilation matrix elements in the `'full_SE'` computation are computed at LO.

[9] In contrast to standard NLL computations, NLL' resumations require that all relevant hard, soft and jet functions are obtained at 1-loop, see e.g. ref. [93].

JHEP02(2024)051

Thus, for a meaningful comparison between the two calculations, a fixed-order expansion of each annihilation matrix element of the `'endp_SE'` calculation must be performed. The LO term of the fixed-order expansion of the IJ-th annihilation matrix element in the `'endp_SE'` calculation should then agree, up to power corrections of $\mathcal{O}(m_W^2/m_\chi^2)$ that are not included in our calculation, with the respective matrix element of the `'full_SE'` computation. Indeed, we find that the annihilation matrix elements associated with the $\chi_1^+\chi_1^- \to \gamma + f\bar{f}$, $\chi_1^+\chi_1^- \to \gamma + Zh$ and $\chi_1^+\chi_1^- \to \gamma + W^+W^-$ processes[10] are exactly reproduced by the expanded results of refs. [91, 92] at the leading order in the power expansion assumed there, and provided that $1 - x \ll 1$. Note that, at LO, the $\gamma + f\bar{f}$ and $\gamma + Zh$ final states can only occur when the initial state is composed of charginos, i.e. these channels only contribute to the diagonal $I = J = \langle 1\bar{1}\rangle$ annihilation matrix element. In contrast, $\gamma + W^+W^-$ final states can also result from neutralino annihilation, which receives contributions also from the $IJ = (\hat{1}\hat{1})(\hat{1}\hat{1})$ and $IJ = (\hat{1}\hat{1})\langle 1\bar{1}\rangle$ combinations.

The agreement between our calculated annihilation matrix elements and those extracted from refs. [91, 92] is very good for masses above the TeV scale, but poor for lighter neutralinos. This is to be expected, as the `'endp_SE'` results are valid only up to power corrections of $\mathcal{O}(m_W^2/m_\chi^2)$ which could be non-negligible for smaller neutralino masses such as $m_\chi = 400\,\text{GeV}$. Our calculations, instead, provide the most accurate and reliable picture for the gamma-ray spectrum from neutralino annihilations in that mass range.

In addition to the comparison with the `'endp_SE'` calculation, we compared our results for the $I = J = (\hat{1}\hat{1})$ annihilation matrix element analytically with the fixed-order neutralino annihilation cross section into a $W^+W^-\gamma$ final state in the pure wino and higgsino limits that has been provided in ref. [86]. We found exact agreement.

5 Conclusions

In this work, we have presented the first calculation of the continuum gamma-ray spectra resulting from neutralino annihilation including the Sommerfeld effect in the MSSM. The main novelty of our work is the systematic inclusion of all combinations of chargino-antichargino and neutralino pair annihilation processes into three-body final states that play a role in the calculation. The impact of the Sommerfeld effect is generically very strong due to the highly non-relativistic nature of the DM particles in the considered scenarios. For the sake of concreteness we focused our numerical discussion on the pure wino and pure higgsino limits of the MSSM. In the neutralino mass range of about 100 GeV to 1 TeV, we find qualitative differences compared to calculations of continuum spectra including only final-state radiation that are traditionally employed in gamma-ray searches for WIMP DM. For neutralinos heavier than about a TeV, the endpoint of the continuum requires the resummation of large Sudakov logarithms from soft/collinear electroweak radiation. Our work fills the gap between previous calculations focusing on the endpoint regime and separate ones for the low-energy photon regime where the widely used final-state radiation approximation is appropriate.

To ensure the correctness of our calculations we performed several stringent consistency checks. We verified that our results agree with older ones in the appropriate limits, we

[10] These are the only calculations of chargino-antichargino annihilation cross sections into three-body final states existing in the literature.

JHEP02(2024)051

checked gauge invariance, unitary safety, and we re-derived the non-relativistic potential for the s-wave annihilation of neutralinos. We also showed that our results are consistent with existing results employing the collinear approximation.

On the technical side, our results will allow for a reassessment of the impact of internal bremsstrahlung by combining it with the Sommerfeld enhancement effect. This will pave the way for robust global fits, especially in reduced-parameter MSSM scenarios. Most importantly, though, our calculation will open the door to detailed phenomenological studies of the indirect detection of neutralinos using gamma-ray observations from *both* satellite and Cherenkov telescopes. In the light of improved energy resolutions and sensitivities of current and next-generation gamma-ray telescopes this is a very timely achievement.

Acknowledgments

We are grateful for valuable discussions to Denys Malyshev and Andrea Santangelo. We would also like to extend our gratitude to Torsten Bringmann and the anonymous referee for their helpful feedback. We acknowledge support by the state of Baden-Württemberg through bwHPC and the German Research Foundation (DFG) through grant no. INST 39/963-1 FUGG (bwForCluster NEMO).

A Conventions

A.1 Neutralino and chargino mixing matrices

All our computations within the MSSM employed the model file `MSSM.mod` that is contained in `FeynArts`. Detailed information about the conventions used in this model file is given in refs. [67, 98–100]. Here, we explicitly denote the elements of the neutralino ($\mathbb{M}_N$) and chargino ($\mathbb{M}_C$) mixing matrices, since these are of immediate relevance for the computations that we present in this work. These are given by

$$\mathbb{M}_N = \begin{pmatrix} M_1 & 0 & -m_Z s_W \cos\beta & m_Z s_W \sin\beta \\ 0 & M_2 & m_Z c_W \cos\beta & -m_Z c_W \sin\beta \\ -m_Z s_W \cos\beta & m_Z c_W \cos\beta & 0 & -\mu \\ m_Z s_W \sin\beta & -m_Z c_W \sin\beta & -\mu & 0 \end{pmatrix}, \tag{A.1}$$

and

$$\mathbb{M}_C = \begin{pmatrix} M_2 & \sqrt{2}\, m_W \sin\beta \\ \sqrt{2}\, m_W \cos\beta & \mu \end{pmatrix}, \tag{A.2}$$

respectively.

The *unitary* mixing matrices $\tilde{N}$, $\tilde{U}$ and $\tilde{V}$ are defined by the following conditions:

$$\tilde{N}^* \mathbb{M}_N \tilde{N}^{-1} = \mathrm{diag}(m_{\chi_1^0}, m_{\chi_2^0}, m_{\chi_3^0}, m_{\chi_4^0}), \; \tilde{U}^* \mathbb{M}_C \tilde{V}^{-1} = \mathrm{diag}(m_{\chi_1^\pm}, m_{\chi_2^\pm}), \tag{A.3}$$

where $m_{\chi_1^0} < m_{\chi_2^0} < m_{\chi_3^0} < m_{\chi_4^0}$ and $m_{\chi_1^0} < m_{\chi_1^\pm} < m_{\chi_2^\pm}$.

JHEP02(2024)051

A.2 Static potential

The potential matrix $V_{IJ}(r)$ for the MSSM given by eq. (3.7) can be decomposed as

$$V_{IJ}(r) = V_{IJ}^{\text{diag}}(r) + V_{IJ}^{\text{off}}(r)\,, \tag{A.4}$$

where

$$\begin{aligned} V_{IJ}^{\text{diag}}(r) &= -\frac{\hat{\alpha}_{IJ}^{\gamma}}{r} - \hat{\alpha}_{IJ}^{Z}\frac{\mathrm{e}^{-m_Z r}}{r} - \hat{\alpha}_{IJ}^{h}\frac{\mathrm{e}^{-m_h r}}{r} - \hat{\alpha}_{IJ}^{H^0}\frac{\mathrm{e}^{-m_{H^0} r}}{r} - \hat{\alpha}_{IJ}^{A^0}\frac{\mathrm{e}^{-m_{A^0} r}}{r}\,, \\ V_{IJ}^{\text{off}}(r) &= -\hat{\alpha}_{IJ}^{W}\frac{\mathrm{e}^{-m_W r}}{r} - \hat{\alpha}_{IJ}^{H^+}\frac{\mathrm{e}^{-m_{H^+} r}}{r}\,. \end{aligned}$$

The coupling matrices $\hat{\alpha}_{IJ}^{B}$ for each mediating boson B are block-diagonal for the neutral mediators $B^0 = \gamma, Z, h, H^0, A^0$ and off-diagonal for the charged bosons $B^+ = W^+, H^+$,

$$\hat{\alpha}_{IJ}^{B^0} = \begin{pmatrix} \hat{\alpha}^{B^0}_{(\hat{i}\hat{j}),(\hat{k}\hat{l})} & \mathbb{O}_{10\times 4} \\ \mathbb{O}_{4\times 10} & \hat{\alpha}^{B^0}_{\langle x\bar{y}\rangle,\langle z\bar{w}\rangle} \end{pmatrix}\,, \qquad \hat{\alpha}_{IJ}^{B^+} = \begin{pmatrix} \mathbb{O}_{10\times 10} & \hat{\alpha}^{B^+}_{(\hat{i}\hat{j}),\langle z\bar{w}\rangle} \\ \hat{\alpha}^{B^+}_{\langle x\bar{y}\rangle,(\hat{k}\hat{l})} & \mathbb{O}_{4\times 4} \end{pmatrix}\,. \tag{A.5}$$

In eqs. (3.9)–(3.14) the coupling matrices have been expressed in terms of the coefficients that are displayed below. In particular, the coefficients associated with massive vector boson interactions are given by

$$v_{ij}^{Z\,(0)} = \frac{1}{2\,c_W}\,\mathrm{Im}\left(N_{i3}N_{j3}^* - N_{i4}N_{j4}^*\right), \qquad a_{ij}^{Z\,(0)} = \frac{1}{2\,c_W}\,\mathrm{Re}\left(N_{i3}N_{j3}^* - N_{i4}N_{j4}^*\right), \tag{A.6}$$

$$v_{xy}^{Z} = -\frac{1}{4c_W}\left(\tilde{U}_{x1}\tilde{U}_{y1}^* + \tilde{V}_{x1}^*\tilde{V}_{y1} + 2(c_W^2 - s_W^2)\delta_{xy}\right), \quad a_{xy}^{Z} = -\frac{1}{4c_W}\left(\tilde{U}_{x1}\tilde{U}_{y1}^* - \tilde{V}_{x1}^*\tilde{V}_{y1}\right), \tag{A.7}$$

$$v_{ix}^{W} = \frac{1}{2}\left[\tilde{N}_{i2}^*\tilde{U}_{x1} + \tilde{N}_{i2}\tilde{V}_{x1}^* + \frac{1}{\sqrt{2}}\left(\tilde{N}_{i3}^*\tilde{U}_{x2} - \tilde{N}_{i4}\tilde{V}_{x2}^*\right)\right], \tag{A.8}$$

$$a_{ix}^{W} = \frac{1}{2}\left[\tilde{N}_{i2}^*\tilde{U}_{x1} - \tilde{N}_{i2}\tilde{V}_{x1}^* + \frac{1}{\sqrt{2}}\left(\tilde{N}_{i3}^*\tilde{U}_{x2} + \tilde{N}_{i4}\tilde{V}_{x2}^*\right)\right], \tag{A.9}$$

where $c_W = \cos\theta_W$ and $s_W = \sin\theta_W$, and the N_{ij}, $\tilde{U}_{ij}$ and $\tilde{V}_{ij}$ denote elements of the unitary mixing matrices defined in eq. (A.3). The coefficients that are associated with charged scalar bosons read

$$\begin{aligned} s_{ix}^{G_W} = &-\frac{1}{2\,c_W}\left[s_\beta\frac{s_W\tilde{N}_{i1}^* + c_W\tilde{N}_{i2}^*}{\sqrt{2}}\tilde{V}_{x2}^* + c_\beta\frac{s_W\tilde{N}_{i1} + c_W\tilde{N}_{i2}}{\sqrt{2}}\tilde{U}_{x2}\right. \\ &\left. - c_\beta c_W\tilde{N}_{i3}\tilde{U}_{x1} + s_\beta c_W\tilde{N}_{i4}^*\tilde{V}_{x1}^*\right], \end{aligned} \tag{A.10}$$

$$\begin{aligned} s_{ix}^{H^+} = &-\frac{1}{2\,c_W}\left[c_\beta\frac{s_W\tilde{N}_{i1}^* + c_W\tilde{N}_{i2}^*}{\sqrt{2}}\tilde{V}_{x2}^* - s_\beta\frac{s_W\tilde{N}_{i1} + c_W\tilde{N}_{i2}}{\sqrt{2}}\tilde{U}_{x2}\right. \\ &\left. + s_\beta c_W\tilde{N}_{i3}\tilde{U}_{x1} + c_\beta c_W\tilde{N}_{i4}^*\tilde{V}_{x1}^*\right], \end{aligned} \tag{A.11}$$

JHEP02(2024)051

where $c_\beta \equiv \cos\beta$ and $s_\beta \equiv \sin\beta$. Finally, the coefficients for the neutral scalar bosons are given by

$$s_{ij}^{G_Z\,(0)} = \frac{i}{4c_W}\left\{[(c_\beta N_{i3} + s_\beta N_{i4})(s_W N_{j1} - c_W N_{j2}) + (i \leftrightarrow j)] - \text{c. c.}\right\}, \tag{A.12}$$

$$s_{ij}^{A_0\,(0)} = -\frac{i}{4c_W}\left\{[(s_\beta N_{i3} - c_\beta N_{i4})(s_W N_{j1} - c_W N_{j2}) + (i \leftrightarrow j)] - \text{c. c.}\right\}, \tag{A.13}$$

$$s_{ij}^{H\,(0)} = \frac{1}{4c_W}\left\{[(c_\alpha N_{i3} - s_\alpha N_{i4})(s_W N_{j1} - c_W N_{j2}) + (i \leftrightarrow j)] + \text{c. c.}\right\}, \tag{A.14}$$

$$s_{ij}^{h\,(0)} = -\frac{1}{4c_W}\left\{[(s_\alpha N_{i3} + c_\alpha N_{i4})(s_W N_{j1} - c_W N_{j2}) + (i \leftrightarrow j)] - \text{c. c.}\right\}, \tag{A.15}$$

$$s_{xy}^{G_Z} = -\frac{i}{2\sqrt{2}}\left[c_\beta(U_{x2}V_{y1} - U_{y2}^* V_{x1}^*) - s_\beta(U_{x1}V_{y2} - U_{y1}^* V_{x2}^*)\right], \tag{A.16}$$

$$s_{xy}^{A_0} = \frac{i}{2\sqrt{2}}\left[s_\beta(U_{x2}V_{y1} - U_{y2}^* V_{x1}^*) + c_\beta(U_{x1}V_{y2} - U_{y1}^* V_{x2}^*)\right], \tag{A.17}$$

$$s_{ij}^{H} = -\frac{1}{2\sqrt{2}}\left[c_\alpha(U_{x2}V_{y1} + U_{y2}^* V_{x1}^*) + s_\alpha(U_{x1}V_{y2} + U_{y1}^* V_{x2}^*)\right], \tag{A.18}$$

$$s_{ij}^{h} = \frac{1}{2\sqrt{2}}\left[s_\alpha(U_{x2}V_{y1} + U_{y2}^* V_{x1}^*) - c_\alpha(U_{x1}V_{y2} + U_{y1}^* V_{x2}^*)\right], \tag{A.19}$$

where $s_\alpha \equiv \sin\tilde{\alpha}$, $c_\alpha \equiv \cos\tilde{\alpha}$ and $\tilde{\alpha}$ is the mixing angle of the CP-even Higgs doublet.

B Parameterization of the three-body phase space

In this work, we consider neutralino and chargino/antichargino pair annihilation processes into three-particle final states of the type $\gamma + X^{(2)}$. The four-momenta of the particles are denoted by k_i with $(i = 1, \ldots 5)$ such that e.g.

$$\chi_x^+(k_1) + \chi_y^-(k_2) \to X_1^{(2)}(k_3) + X_2^{(2)}(k_4) + \gamma(k_5)\,, \tag{B.1}$$

with the $X_{1,2}^{(2)}$ denoting the two final-state particles resulting from the $X^{(2)}$ system.

The non-relativistic initial-state particles are assumed to be at rest, i.e. $k_1 = (m_\chi, \vec{0})^T$ and $k_2 = (m_\chi, \vec{0})^T$. Assuming that the photon propagates along the z axis we find $k_5^0 = ||\vec{k}_5|| = m_\chi x = m_\chi - \frac{s_{34}}{4m_\chi}$, with $s_{34} = m_X^2 = (k_3 + k_4)^2 = 4m_\chi^2(1-x)$, where m_X is the invariant mass of the subsystem $X^{(2)}$ of the final state in a $2 \to 3$ scattering process of type $\chi_x^+\chi_y^- \to \gamma + X^{(2)}$. We choose a reference system where $\vec{k}_3$ and $\vec{k}_4$ are lying in the yz plane ($k_3^x = k_4^x = 0$). The components of k_3^μ are given by

$$k_3^0 = \frac{m_\chi}{2z}\left[(1+z)\left(z - \frac{m_4^2 - m_3^2}{4m_\chi^2}\right) - (1-z)\sqrt{z - \left(\frac{m_4 - m_3}{2m_\chi}\right)^2}\sqrt{z - \left(\frac{m_4 + m_3}{2m_\chi}\right)^2}\cos\theta_3^*\right],$$

$$k_3^y = -\,k_4^y = \frac{m_\chi}{\sqrt{z}}\sqrt{z - \left(\frac{m_4 - m_3}{2m_\chi}\right)^2}\sqrt{z - \left(\frac{m_4 + m_3}{2m_\chi}\right)^2}\sin\theta_3^*\,,$$

$$k_3^z = -\,\frac{m_\chi}{2z}\left[(1-z)\left(z - \frac{m_4^2 - m_3^2}{4m_\chi^2}\right) - (1+z)\sqrt{z - \left(\frac{m_4 - m_3}{2m_\chi}\right)^2}\sqrt{z - \left(\frac{m_4 + m_3}{2m_\chi}\right)^2}\cos\theta_3^*\right],$$

JHEP02(2024)051

where $z = 1 - x$ with $x = E_\gamma/m_\chi$; θ_3^* (θ_4^*) is the relative angle between k_3 (k_4) and k_5 in the rest frame of $X^{(2)}$. The components of k_4 are obtained by interchanging m_3, θ_3^* with m_4 and θ_4^* in the expressions for k_3 above. The three-particle phase space can thus be fully parametrized by the variables x and θ_3^*.

The annihilation matrix elements of eq. (3.15) in this parametrization are given by

$$\left[\frac{\mathrm{d}(\tilde{\sigma v})}{\mathrm{d}E_\gamma}\right]_{IJ} = \frac{1}{(\sqrt{2})^{\mathrm{id}(I)+\mathrm{id}(J)}} \sum_{X^{(2)}} \frac{x\lambda\left[4\,m_\chi^2(1-x), m_3^2, m_4^2\right]}{(16\,\pi)^3 m_\chi^3 (1-x)} \times \int_{-1}^{1} \mathrm{d}(\cos\theta_3^*) \mathcal{A}^{(\ell,s)=(0,0)\,*}_{J\to\gamma+X^{(2)}} \mathcal{A}^{(\ell,s)=(0,0)}_{I\to\gamma+X^{(2)}}\,, \tag{B.2}$$

where $\lambda[a,b,c] = \sqrt{a^2+b^2+c^2-2ab-2ac-2bc}$. In our generic notation the summation over all possible spin and helicity configurations of the final-state particles is implied in the summation over $X^{(2)}$.

As discussed in section 3, the amplitudes $\mathcal{A}^{(\ell,s)=(0,0)}_{I\to\gamma+X^{(2)}}$ are obtained by projecting the (standard) amplitude for individual spins $\mathcal{A}(\chi_x^+(s_1)\chi_y^-(s_2)\to\gamma(\lambda_5)+X^{(2)})$ ($\lambda_5 = \pm 1$ is the photon helicity) that is generated by `FeynArts` and `FeynCalc` onto the s-wave $(\ell, s) = (0,0)$ state that is relevant for formula (B.2):

$$\mathcal{A}^{(\ell,s)=(0,0)}_{I\to\gamma+X^{(2)}} = \frac{1}{\sqrt{2}}\left(\mathcal{A}(\chi_x^+(\uparrow)\chi_y^-(\downarrow)\to\gamma+X^{(2)}) - \mathcal{A}(\chi_x^+(\downarrow)\chi_y^-(\uparrow)\to\gamma+X^{(2)})\right) \tag{B.3}$$

The `FeynArts` and `FeynCalc` expressions depend on both the $u(k_i, s_i)$ and $v(k_i, s_i)$ ($i = 1, 2$) spinors of the incoming fermions. Using the z axis as the reference axis, in the Weyl representation these spinors are given by

$$u(k_i, s_i) = \sqrt{m_\chi}\begin{pmatrix} \frac{1}{2}+s_i \\ \frac{1}{2}-s_i \\ \frac{1}{2}+s_i \\ \frac{1}{2}-s_i \end{pmatrix}\quad,\quad v(k_i, s_i) = \sqrt{m_\chi}\begin{pmatrix} -\frac{1}{2}+s_i \\ \frac{1}{2}+s_i \\ \frac{1}{2}-s_i \\ -\frac{1}{2}-s_i \end{pmatrix}\,. \tag{B.4}$$

B.1 Final state parameterizations

B.1.1 Final states including vector bosons: $W^+W^-\gamma$, $W^\pm H^\mp\gamma$, $ZS\gamma$

The polarization vector of the photon is given by $\varepsilon^\gamma(\lambda_5) = (0, -1/\sqrt{2}, i\lambda_5/\sqrt{2}, 0)^T$. For final states with massive gauge bosons the corresponding polarization vectors are given by

$$\varepsilon^V(k_i, \lambda_i \neq 0) = \begin{pmatrix} -\frac{i(1-z)\sin\theta_3^*}{2\sqrt{2z}} \\ \frac{\lambda_i}{\sqrt{2}} \\ -\frac{i\cos\theta_3^*}{\sqrt{2}} \\ \frac{i(1+z)\sin\theta_3^*}{2\sqrt{2z}} \end{pmatrix}\,, \tag{B.5}$$

JHEP02(2024)051

for $\lambda_i = \pm 1$ and

$$\varepsilon^V(k_3, \lambda_3 = 0) = \frac{1}{4m_3 m_\chi z} \begin{pmatrix} \lambda(4m_\chi^2 z, m_3^2, m_4^2)(1+z) - (4m_\chi^2 z + m_3^2 - m_4^2)(1-z) \\ 0 \\ \sqrt{z}(4m_\chi^2 z + m_3^2 - m_4^2)\sin\theta_3^* \\ -\lambda(4m_\chi^2 z, m_3^2, m_4^2)(1-z) + (4m_\chi^2 z + m_3^2 - m_4^2)(1+z) \end{pmatrix}, \tag{B.6}$$

for $\lambda_3 = 0$. For the $W^+W^-\gamma$ case the polarization vector $\varepsilon(k_4, \lambda_4 = 0)$ is obtained by interchanging m_3, θ_3^* with m_4 and θ_4^* respectively. For the $W^\pm H^\mp\gamma$, $ZS\gamma$ final states, we use the polarization vectors above (as functions of k_3, λ_3) for the massive gauge boson and assume that the scalar particle has 4-momentum k_4.

B.1.2 Final states with fermions: $\bar{q}q\gamma$, $l^+l^-\gamma$, $\nu\bar{\nu}\gamma$

The final-state spinors for (anti-)fermions f with mass m_f and helicities s_3, s_4, are given by

$$u_f(k_3, s_3) = \begin{pmatrix} \left(\frac{1}{2} + s_3\right)\sqrt{m_\chi - \sqrt{m_\chi^2 z - m_f^2}\frac{\cos\theta_3^*}{\sqrt{z}}} \\ \frac{\left(\frac{1}{2} - s_3\right)m_f - i\left(\frac{1}{2} + s_3\right)\sqrt{m_\chi^2 z - m_f^2}\sin\theta_3^*}{\sqrt{m_\chi - \sqrt{m_\chi^2 z - m_f^2}\frac{\cos\theta_3^*}{\sqrt{z}}}} \\ \frac{\left(\frac{1}{2} + s_3\right)m_f - i\left(\frac{1}{2} - s_3\right)\sqrt{m_\chi^2 z - m_f^2}\sin\theta_3^*}{\sqrt{m_\chi - \sqrt{m_\chi^2 z - m_f^2}\frac{\cos\theta_3^*}{\sqrt{z}}}} \\ \left(\frac{1}{2} - s_3\right)\sqrt{m_\chi - \sqrt{m_\chi^2 z - m_f^2}\frac{\cos\theta_3^*}{\sqrt{z}}} \end{pmatrix}, \tag{B.7}$$

and

$$v_{\bar{f}}(k_4, s_4) = \begin{pmatrix} -\left(\frac{1}{2} - s_4\right)\sqrt{m_\chi + \sqrt{m_\chi^2 z - m_f^2}\frac{\cos\theta_3^*}{\sqrt{z}}} \\ \frac{\left(\frac{1}{2} + s_4\right)m_f - i\left(\frac{1}{2} - s_4\right)\sqrt{m_\chi^2 z - m_f^2}\sin\theta_3^*}{\sqrt{m_\chi + \sqrt{m_\chi^2 z - m_f^2}\frac{\cos\theta_3^*}{\sqrt{z}}}} \\ \frac{\left(\frac{1}{2} - s_4\right)m_f - i\left(\frac{1}{2} + s_4\right)\sqrt{m_\chi^2 z - m_f^2}\sin\theta_3^*}{\sqrt{m_\chi + \sqrt{m_\chi^2 z - m_f^2}\frac{\cos\theta_3^*}{\sqrt{z}}}} \\ -\left(\frac{1}{2} + s_4\right)\sqrt{m_\chi + \sqrt{m_\chi^2 z - m_f^2}\frac{\cos\theta_3^*}{\sqrt{z}}} \end{pmatrix}. \tag{B.8}$$

References

[1] N. Arkani-Hamed and S. Dimopoulos, *Supersymmetric unification without low energy supersymmetry and signatures for fine-tuning at the LHC*, *JHEP* **06** (2005) 073 [hep-th/0405159] [INSPIRE].

JHEP02(2024)051

[2] G.F. Giudice and A. Romanino, *Split supersymmetry*, *Nucl. Phys. B* **699** (2004) 65 [hep-ph/0406088] [INSPIRE].

[3] J.D. Wells, *PeV-scale supersymmetry*, *Phys. Rev. D* **71** (2005) 015013 [hep-ph/0411041] [INSPIRE].

[4] N. Arkani-Hamed, A. Delgado and G.F. Giudice, *The Well-tempered neutralino*, *Nucl. Phys. B* **741** (2006) 108 [hep-ph/0601041] [INSPIRE].

[5] ATLAS collaboration, *Search for chargino–neutralino pair production in final states with three leptons and missing transverse momentum in* $\sqrt{s} = 13$ *TeV pp collisions with the ATLAS detector*, *Eur. Phys. J. C* **81** (2021) 1118 [arXiv:2106.01676] [INSPIRE].

[6] CMS collaboration, *Search for supersymmetry in final states with two oppositely charged same-flavor leptons and missing transverse momentum in proton-proton collisions at* $\sqrt{s} = 13$ *TeV*, *JHEP* **04** (2021) 123 [arXiv:2012.08600] [INSPIRE].

[7] XENON collaboration, *First Dark Matter Search with Nuclear Recoils from the XENONnT Experiment*, *Phys. Rev. Lett.* **131** (2023) 041003 [arXiv:2303.14729] [INSPIRE].

[8] LZ collaboration, *First Dark Matter Search Results from the LUX-ZEPLIN (LZ) Experiment*, *Phys. Rev. Lett.* **131** (2023) 041002 [arXiv:2207.03764] [INSPIRE].

[9] CRESST collaboration, *First results from the CRESST-III low-mass dark matter program*, *Phys. Rev. D* **100** (2019) 102002 [arXiv:1904.00498] [INSPIRE].

[10] XENON collaboration, *The XENON1T Dark Matter Experiment*, *Eur. Phys. J. C* **77** (2017) 881 [arXiv:1708.07051] [INSPIRE].

[11] Y.B. Zeldovich, A.A. Klypin, M.Y. Khlopov and V.M. Chechetkin, *Astrophysical constraints on the mass of heavy stable neutral leptons*, *Sov. J. Nucl. Phys.* **31** (1980) 664 [INSPIRE].

[12] G. Jungman, M. Kamionkowski and K. Griest, *Supersymmetric dark matter*, *Phys. Rept.* **267** (1996) 195 [hep-ph/9506380] [INSPIRE].

[13] A. Sommerfeld, *Über die Beugung und Bremsung der Elektronen*, *Annalen Phys.* **403** (1931) 257 [INSPIRE].

[14] G. Gamow, *Zur Quantentheorie des Atomkernes*, *Z. Phys.* **51** (1928) 204 [INSPIRE].

[15] A.D. Sakharov, *Interaction of an Electron and Positron in Pair Production*, *Zh. Eksp. Teor. Fiz.* **18** (1948) 631 [INSPIRE].

[16] FERMI-LAT collaboration, *The Large Area Telescope on the Fermi Gamma-ray Space Telescope Mission*, *Astrophys. J.* **697** (2009) 1071 [arXiv:0902.1089] [INSPIRE].

[17] H.E.S.S. collaboration, *Observations of the Crab Nebula with H.E.S.S*, *Astron. Astrophys.* **457** (2006) 899 [astro-ph/0607333] [INSPIRE].

[18] VERITAS collaboration, *The first VERITAS telescope*, *Astropart. Phys.* **25** (2006) 391 [astro-ph/0604119] [INSPIRE].

[19] MAGIC collaboration, *The major upgrade of the MAGIC telescopes, Part II: A performance study using observations of the Crab Nebula*, *Astropart. Phys.* **72** (2016) 76 [arXiv:1409.5594] [INSPIRE].

[20] CTA CONSORTIUM collaboration, *Design concepts for the Cherenkov Telescope Array CTA: An advanced facility for ground-based high-energy gamma-ray astronomy*, *Exper. Astron.* **32** (2011) 193 [arXiv:1008.3703] [INSPIRE].

JHEP02(2024)051

[21] LHAASO collaboration, *The Large High Altitude Air Shower Observatory (LHAASO) Science Book (2021 Edition)*, *Chin. Phys. C* **46** (2022) 035001 [arXiv:1905.02773] [INSPIRE].

[22] HAWC collaboration, *The HAWC observatory*, *Nucl. Instrum. Meth. A* **692** (2012) 72 [INSPIRE].

[23] M. Beneke et al., *The last refuge of mixed wino-Higgsino dark matter*, *JHEP* **01** (2017) 002 [arXiv:1611.00804] [INSPIRE].

[24] GAMBIT collaboration, *A global fit of the MSSM with GAMBIT*, *Eur. Phys. J. C* **77** (2017) 879 [arXiv:1705.07917] [INSPIRE].

[25] GAMBIT collaboration, *Global fits of GUT-scale SUSY models with GAMBIT*, *Eur. Phys. J. C* **77** (2017) 824 [arXiv:1705.07935] [INSPIRE].

[26] A. Hryczuk et al., *Testing dark matter with Cherenkov light — prospects of H.E.S.S. and CTA for exploring minimal supersymmetry*, *JHEP* **10** (2019) 043 [arXiv:1905.00315] [INSPIRE].

[27] J. Ellis, K.A. Olive, V.C. Spanos and I.D. Stamou, *The CMSSM survives Planck, the LHC, LUX-ZEPLIN, Fermi-LAT, H.E.S.S. and IceCube*, *Eur. Phys. J. C* **83** (2023) 246 [arXiv:2210.16337] [INSPIRE].

[28] G. Arcadi et al., *The hMSSM with a light gaugino/higgsino sector: implications for collider and astroparticle physics*, *JHEP* **05** (2023) 095 [arXiv:2206.11881] [INSPIRE].

[29] J.W. Foster et al., *Search for dark matter lines at the Galactic Center with 14 years of Fermi data*, *Phys. Rev. D* **107** (2023) 103047 [arXiv:2212.07435] [INSPIRE].

[30] FERMI-LAT collaboration, *Searching for Dark Matter Annihilation from Milky Way Dwarf Spheroidal Galaxies with Six Years of Fermi Large Area Telescope Data*, *Phys. Rev. Lett.* **115** (2015) 231301 [arXiv:1503.02641] [INSPIRE].

[31] MAGIC and FERMI-LAT collaborations, *Limits to Dark Matter Annihilation Cross-Section from a Combined Analysis of MAGIC and Fermi-LAT Observations of Dwarf Satellite Galaxies*, *JCAP* **02** (2016) 039 [arXiv:1601.06590] [INSPIRE].

[32] HAWC collaboration, *Dark Matter Limits From Dwarf Spheroidal Galaxies with The HAWC Gamma-Ray Observatory*, *Astrophys. J.* **853** (2018) 154 [arXiv:1706.01277] [INSPIRE].

[33] HESS collaboration, *Searches for gamma-ray lines and 'pure WIMP' spectra from Dark Matter annihilations in dwarf galaxies with H.E.S.S*, *JCAP* **11** (2018) 037 [arXiv:1810.00995] [INSPIRE].

[34] VERITAS collaboration, *Dark Matter Constraints from a Joint Analysis of Dwarf Spheroidal Galaxy Observations with VERITAS*, *Phys. Rev. D* **95** (2017) 082001 [arXiv:1703.04937] [INSPIRE].

[35] M. Michailidis et al., *Prospects for annihilating dark matter from M31 and M33 observations with the Cherenkov Telescope Array*, *JCAP* **08** (2023) 073 [arXiv:2304.08202] [INSPIRE].

[36] J. Hisano, S. Matsumoto and M.M. Nojiri, *Explosive dark matter annihilation*, *Phys. Rev. Lett.* **92** (2004) 031303 [hep-ph/0307216] [INSPIRE].

[37] L. Bergstrom, P. Ullio and J.H. Buckley, *Observability of gamma-rays from dark matter neutralino annihilations in the Milky Way halo*, *Astropart. Phys.* **9** (1998) 137 [astro-ph/9712318] [INSPIRE].

[38] L. Pieri, J. Lavalle, G. Bertone and E. Branchini, *Implications of High-Resolution Simulations on Indirect Dark Matter Searches*, *Phys. Rev. D* **83** (2011) 023518 [arXiv:0908.0195] [INSPIRE].

JHEP02(2024)051

[39] P.J. McMillan, *Mass models of the Milky Way*, *Mon. Not. Roy. Astron. Soc.* **414** (2011) 2446 [arXiv:1102.4340] [INSPIRE].

[40] F. Iocco, M. Pato, G. Bertone and P. Jetzer, *Dark Matter distribution in the Milky Way: microlensing and dynamical constraints*, *JCAP* **11** (2011) 029 [arXiv:1107.5810] [INSPIRE].

[41] G.D. Martinez, *A robust determination of Milky Way satellite properties using hierarchical mass modelling*, *Mon. Not. Roy. Astron. Soc.* **451** (2015) 2524 [arXiv:1309.2641] [INSPIRE].

[42] A. Geringer-Sameth, S.M. Koushiappas and M. Walker, *Dwarf galaxy annihilation and decay emission profiles for dark matter experiments*, *Astrophys. J.* **801** (2015) 74 [arXiv:1408.0002] [INSPIRE].

[43] R. Gavazzi et al., *A weak lensing study of the Coma cluster*, *Astron. Astrophys.* **498** (2009) L33 [arXiv:0904.0220] [INSPIRE].

[44] C. Bierlich et al., *A comprehensive guide to the physics and usage of PYTHIA 8.3*, *SciPost Phys. Codeb.* **2022** (2022) 8 [arXiv:2203.11601] [INSPIRE].

[45] J. Bellm et al., *Herwig 7.0/Herwig++ 3.0 release note*, *Eur. Phys. J. C* **76** (2016) 196 [arXiv:1512.01178] [INSPIRE].

[46] T. Bringmann et al., *DarkSUSY 6: An Advanced Tool to Compute Dark Matter Properties Numerically*, *JCAP* **07** (2018) 033 [arXiv:1802.03399] [INSPIRE].

[47] M. Cirelli et al., *PPPC 4 DM ID: A Poor Particle Physicist Cookbook for Dark Matter Indirect Detection*, *JCAP* **03** (2011) 051 [*Erratum ibid.* **10** (2012) E01] [arXiv:1012.4515] [INSPIRE].

[48] G. Belanger et al., *Indirect search for dark matter with micrOMEGAs2.4*, *Comput. Phys. Commun.* **182** (2011) 842 [arXiv:1004.1092] [INSPIRE].

[49] P. Gondolo et al., *DarkSUSY: Computing supersymmetric dark matter properties numerically*, *JCAP* **07** (2004) 008 [astro-ph/0406204] [INSPIRE].

[50] P. Ciafaloni et al., *Weak Corrections are Relevant for Dark Matter Indirect Detection*, *JCAP* **03** (2011) 019 [arXiv:1009.0224] [INSPIRE].

[51] L. Bergstrom, *Radiative Processes in Dark Matter Photino Annihilation*, *Phys. Lett. B* **225** (1989) 372 [INSPIRE].

[52] R. Flores, K.A. Olive and S. Rudaz, *Radiative Processes in Lsp Annihilation*, *Phys. Lett. B* **232** (1989) 377 [INSPIRE].

[53] E.A. Baltz and L. Bergstrom, *Detection of leptonic dark matter*, *Phys. Rev. D* **67** (2003) 043516 [hep-ph/0211325] [INSPIRE].

[54] T. Bringmann, L. Bergstrom and J. Edsjo, *New Gamma-Ray Contributions to Supersymmetric Dark Matter Annihilation*, *JHEP* **01** (2008) 049 [arXiv:0710.3169] [INSPIRE].

[55] V. Barger, Y. Gao, W.Y. Keung and D. Marfatia, *Generic dark matter signature for gamma-ray telescopes*, *Phys. Rev. D* **80** (2009) 063537 [arXiv:0906.3009] [INSPIRE].

[56] N.F. Bell et al., *W/Z Bremsstrahlung as the Dominant Annihilation Channel for Dark Matter, Revisited*, *Phys. Lett. B* **706** (2011) 6 [arXiv:1104.3823] [INSPIRE].

[57] M. Garny, A. Ibarra and S. Vogl, *Antiproton constraints on dark matter annihilations from internal electroweak bremsstrahlung*, *JCAP* **07** (2011) 028 [arXiv:1105.5367] [INSPIRE].

[58] T. Bringmann, F. Calore, A. Galea and M. Garny, *Electroweak and Higgs Boson Internal Bremsstrahlung: General considerations for Majorana dark matter annihilation and application to MSSM neutralinos*, *JHEP* **09** (2017) 041 [arXiv:1705.03466] [INSPIRE].

JHEP02(2024)051

[59] J. Hisano, S. Matsumoto and M.M. Nojiri, *Unitarity and higher order corrections in neutralino dark matter annihilation into two photons*, *Phys. Rev. D* **67** (2003) 075014 [hep-ph/0212022] [INSPIRE].

[60] J. Hisano, S. Matsumoto, M.M. Nojiri and O. Saito, *Non-perturbative effect on dark matter annihilation and gamma ray signature from galactic center*, *Phys. Rev. D* **71** (2005) 063528 [hep-ph/0412403] [INSPIRE].

[61] G.T. Bodwin, E. Braaten and G.P. Lepage, *Rigorous QCD analysis of inclusive annihilation and production of heavy quarkonium*, *Phys. Rev. D* **51** (1995) 1125 [*Erratum ibid.* **55** (1997) 5853] [hep-ph/9407339] [INSPIRE].

[62] M. Beneke, C. Hellmann and P. Ruiz-Femenia, *Non-relativistic pair annihilation of nearly mass degenerate neutralinos and charginos I. General framework and S-wave annihilation*, *JHEP* **03** (2013) 148 [*Erratum ibid.* **10** (2013) 224] [arXiv:1210.7928] [INSPIRE].

[63] C. Hellmann and P. Ruiz-Femenía, *Non-relativistic pair annihilation of nearly mass degenerate neutralinos and charginos II. P-wave and next-to-next-to-leading order S-wave coefficients*, *JHEP* **08** (2013) 084 [arXiv:1303.0200] [INSPIRE].

[64] M. Beneke, C. Hellmann and P. Ruiz-Femenia, *Non-relativistic pair annihilation of nearly mass degenerate neutralinos and charginos III. Computation of the Sommerfeld enhancements*, *JHEP* **05** (2015) 115 [arXiv:1411.6924] [INSPIRE].

[65] M. Beneke, A. Broggio, C. Hasner and M. Vollmann, *Energetic γ-rays from TeV scale dark matter annihilation resummed*, *Phys. Lett. B* **786** (2018) 347 [*Erratum ibid.* **810** (2020) 135831] [arXiv:1805.07367] [INSPIRE].

[66] M. Beneke, S. Lederer and C. Peset, *Electroweak resummation of neutralino dark-matter annihilation into high-energy photons*, *JHEP* **01** (2023) 171 [arXiv:2211.14341] [INSPIRE].

[67] T. Hahn and C. Schappacher, *The Implementation of the minimal supersymmetric standard model in FeynArts and FormCalc*, *Comput. Phys. Commun.* **143** (2002) 54 [hep-ph/0105349] [INSPIRE].

[68] Wolfram Inc., *Mathematica*, Version 13.3.

[69] T. Hahn, *Generating Feynman diagrams and amplitudes with FeynArts 3*, *Comput. Phys. Commun.* **140** (2001) 418 [hep-ph/0012260] [INSPIRE].

[70] T. Hahn and M. Pérez-Victoria, *Automatized one loop calculations in four-dimensions and D-dimensions*, *Comput. Phys. Commun.* **118** (1999) 153 [hep-ph/9807565] [INSPIRE].

[71] T. Hahn, S. Paßehr and C. Schappacher, *FormCalc 9 and Extensions*, *PoS* **LL2016** (2016) 068 [arXiv:1604.04611] [INSPIRE].

[72] M. Cirelli, N. Fornengo and A. Strumia, *Minimal dark matter*, *Nucl. Phys. B* **753** (2006) 178 [hep-ph/0512090] [INSPIRE].

[73] T. Cohen, M. Lisanti, A. Pierce and T.R. Slatyer, *Wino Dark Matter Under Siege*, *JCAP* **10** (2013) 061 [arXiv:1307.4082] [INSPIRE].

[74] J.J. Fan and M. Reece, *In Wino Veritas? Indirect Searches Shed Light on Neutralino Dark Matter*, *JHEP* **10** (2013) 124 [arXiv:1307.4400] [INSPIRE].

[75] L. Rinchiuso et al., *Prospects for detecting heavy WIMP dark matter with the Cherenkov Telescope Array: The Wino and Higgsino*, *Phys. Rev. D* **103** (2021) 023011 [arXiv:2008.00692] [INSPIRE].

JHEP02(2024)051

[76] C. Dessert et al., *Higgsino Dark Matter Confronts 14 Years of Fermi γ-Ray Data*, *Phys. Rev. Lett.* **130** (2023) 201001 [arXiv:2207.10090] [INSPIRE].

[77] S. Dimopoulos and D.W. Sutter, *The Supersymmetric flavor problem*, *Nucl. Phys. B* **452** (1995) 496 [hep-ph/9504415] [INSPIRE].

[78] MSSM Working Group collaboration, *The Minimal supersymmetric standard model: Group summary report*, in the proceedings of the *GDR (Groupement De Recherche) — Supersymetrie*, Montpellier, France (1998) [hep-ph/9901246] [INSPIRE].

[79] G.L. Kane, C.F. Kolda, L. Roszkowski and J.D. Wells, *Study of constrained minimal supersymmetry*, *Phys. Rev. D* **49** (1994) 6173 [hep-ph/9312272] [INSPIRE].

[80] S. Bottaro et al., *Closing the window on WIMP Dark Matter*, *Eur. Phys. J. C* **82** (2022) 31 [arXiv:2107.09688] [INSPIRE].

[81] S. Bottaro et al., *The last complex WIMPs standing*, *Eur. Phys. J. C* **82** (2022) 992 [arXiv:2205.04486] [INSPIRE].

[82] Particle Data Group collaboration, *Review of Particle Physics*, *PTEP* **2022** (2022) 083C01 [INSPIRE].

[83] N. Arkani-Hamed, D.P. Finkbeiner, T.R. Slatyer and N. Weiner, *A Theory of Dark Matter*, *Phys. Rev. D* **79** (2009) 015014 [arXiv:0810.0713] [INSPIRE].

[84] M. Ibe, S. Matsumoto and R. Sato, *Mass Splitting between Charged and Neutral Winos at Two-Loop Level*, *Phys. Lett. B* **721** (2013) 252 [arXiv:1212.5989] [INSPIRE].

[85] M. Beneke, C. Hasner, K. Urban and M. Vollmann, *Precise yield of high-energy photons from Higgsino dark matter annihilation*, *JHEP* **03** (2020) 030 [arXiv:1912.02034] [INSPIRE].

[86] L. Bergstrom, T. Bringmann, M. Eriksson and M. Gustafsson, *Gamma rays from heavy neutralino dark matter*, *Phys. Rev. Lett.* **95** (2005) 241301 [hep-ph/0507229] [INSPIRE].

[87] L. Bergstrom and P. Ullio, *Full one loop calculation of neutralino annihilation into two photons*, *Nucl. Phys. B* **504** (1997) 27 [hep-ph/9706232] [INSPIRE].

[88] P. Ullio and L. Bergstrom, *Neutralino annihilation into a photon and a Z boson*, *Phys. Rev. D* **57** (1998) 1962 [hep-ph/9707333] [INSPIRE].

[89] K. Urban, *NLO electroweak potentials for minimal dark matter and beyond*, *JHEP* **10** (2021) 136 [arXiv:2108.07285] [INSPIRE].

[90] E.J. Chun, J.-C. Park and S. Scopel, *Non-perturbative Effect and PAMELA Limit on Electro-Weak Dark Matter*, *JCAP* **12** (2012) 022 [arXiv:1210.6104] [INSPIRE].

[91] M. Beneke et al., *Resummed photon spectrum from dark matter annihilation for intermediate and narrow energy resolution*, *JHEP* **08** (2019) 103 [*Erratum ibid.* **07** (2020) 145] [arXiv:1903.08702] [INSPIRE].

[92] M. Beneke, K. Urban and M. Vollmann, *Matching resummed endpoint and continuum γ-ray spectra from dark-matter annihilation*, *Phys. Lett. B* **834** (2022) 137248 [arXiv:2203.01692] [INSPIRE].

[93] T. Becher, A. Broggio and A. Ferroglia, *Introduction to Soft-Collinear Effective Theory*, Springer (2015) [DOI:10.1007/978-3-319-14848-9] [INSPIRE].

[94] M. Vollmann, *Resummation of large electroweak terms for indirect dark matter detection*, in the proceedings of the *Strong interactions from QCD to new strong dynamics at LHC and Future Colliders*, Trento, Italy (2022), pg. 79 [INSPIRE].

JHEP02(2024)051

[95] M. Baumgart et al., *Resummed Photon Spectra for WIMP Annihilation*, *JHEP* **03** (2018) 117 [arXiv:1712.07656] [INSPIRE].

[96] M. Baumgart et al., *Precision Photon Spectra for Wino Annihilation*, *JHEP* **01** (2019) 036 [arXiv:1808.08956] [INSPIRE].

[97] M. Baumgart and V. Vaidya, *Semi-inclusive wino and higgsino annihilation to LL'*, *JHEP* **03** (2016) 213 [arXiv:1510.02470] [INSPIRE].

[98] H.E. Haber and G.L. Kane, *The Search for Supersymmetry: Probing Physics Beyond the Standard Model*, *Phys. Rept.* **117** (1985) 75 [INSPIRE].

[99] J.F. Gunion and H.E. Haber, *Higgs Bosons in Supersymmetric Models. 1.*, *Nucl. Phys. B* **272** (1986) 1 [INSPIRE].

[100] J.F. Gunion and H.E. Haber, *Higgs Bosons in Supersymmetric Models. 2. Implications for Phenomenology*, *Nucl. Phys. B* **278** (1986) 449 [INSPIRE].

JHEP02(2024)051